NUMERICAL ANALYSIS OF POROUS SOLIDS

NUMERICAL ANALYSIS OF POROUS SOLIDS

By

MAJID TAHERKHANI, B.Eng

A Project
Submitted to the School of Graduate Studies
in Partial Fulfilment of the Requirements
for the Degree
Master of Engineering

McMaster University

MASTER OF ENGINEERING (Civil Engineering)

McMASTER UNIVERSITY
Hamilton, Ontario
Canada

TITLE: Numerical Analysis of Porous Solids

AUTHOR: Majid Taherkhani
B. Eng. (Tehran Polytechnic University, Tehran, Iran)

SUPERVISOR: Professor S. Pietruszczak

NUMBER OF PAGES: x, 111

ABSTRACT

The main objective of this project is to study the mechanical behaviour of anisotropic porous solids. The mechanical response of this class of materials depends on porosity, which is a primary factor affecting the mechanical characteristics. The other parameters that are commonly used to describe the orientation of material's microstructure are known as fabric tensors. Fabric tensors characterize the arrangement of the microstructural components in a porous material. The concept of fabric tensors is employed to define the constitutive equations and the corresponding failure criteria of porous solids. The presence of liquid in a porous solid can influence the mechanical properties. When the material is in compression the deformation process is constrained and the mechanical behaviour is different from that observed in the dry material. This effect has also been investigated.

To illustrate the performance of the formulation, a numerical analysis of the fracture in proximal femur due to a sideways fall was performed. The analysis incorporated a finite element model developed in the work of Pietruszczak et al.(1999a), in which the geometry of femur was extracted from CT scans. The numerical study in this project extends the previous work in two major areas. First, a static analysis was performed, taking into the account the biphasic nature of the bone material. The second contribution concerns the extension of the analysis to dynamic range, which simulates more closely the condition of a sideways fall.

Acknowledgements

The author wishes to express his sincerest gratitude and deepest appreciation to his supervisor, Dr. S. Pietruszczak, for his constant advice, criticism, and encouragement throughout the research and preparation of this thesis.

The author wishes to extend his appreciation to numerous colleagues and friends for their constant encouragement and sharing information.

The financial support from the Department of Civil Engineering, McMaster University is gratefully acknowledged.

Finally, this thesis is dedicated to my parents in appreciation of their support and encouragement throughout the duration of this study.

TABLE OF CONTENTS

LIST OF FIGURES

Chapter 1

INTRODUCTION

1.1-General remarks

A porous solid consists of an interconnected network of solid particles or, in other words, an assembly of particles with solid edges or faces, packed together so that they fill space. Examples of such material that are common in nature include wood, cork, coral, cancellous bone, etc.

Man has made use of natural porous materials for centuries. The pyramids of Egypt have yielded wooden artifacts at least 5000 years old and cork was used for bungs in wine bottles as far back as Roman times (Gibson,1988). At the simplest level, there are honeycomb-like materials which consist of parallel prismatic cells that are used for lightweight structural components. More common, however, are polymeric foams used in products that range from disposable coffee cups to the crash padding of an aircraft cockpit. The newer foams are increasingly used for insulation and in systems for absorbing the kinetic energy from impact. Their uses exploit the unique combination of properties which are ultimately derived from their cellular structure.

Many porous materials support static and cyclic loads for a long period of time. The structural use of these materials is very old . Wood, for example, is still the world's most widely used component in engineering construction. Our understanding of the way in which its properties depend on the density and on the direction of loading can lead to improved design. Interest in the mechanics of cancellous bone stems from the need to understand bone fracture mechanisms and bone diseases as well as from an attempt to create material which can replace damaged bone. In addition, many different uses of concrete in structures around the world require a deep understanding of it's mechanical properties and behavior in varying conditions.

The microstructure of porous solids ranges from the near perfect order of the bee's honeycomb to the disordered, three dimensional networks of sponges and foams as can be seen the Fig(1.1).

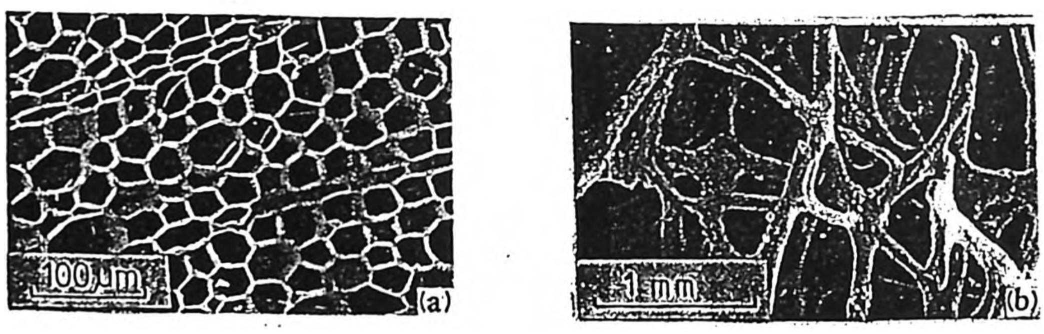

Fig.(1.1)
a) balsa and b) cancellous bone (From: Gibson,1988)

At first sight, one might suppose that the cell size should be an important parameter, and sometimes it is. However, most mechanical and thermal properties depend only partially on cell size, with cell shape being a more important variable. For example, when the cells are equiaxed the properties are *isotropic*, whereas when cells are even slightly elongated or flattened the properties are orientation dependent, often strongly, and are *orthotropic.*

Another important structural characteristic of a porous solid is *porosity,* which can be defined as the ratio of the volume of voids to the volume of solids. Porosity has significant effect in defining mechanical properties. Density and stiffness as well as stress field and failure criteria are all dependent on porosity. It is important to distinguish between two kinds of void space: one which forms a continuous phase within the porous material, called interconnected or "*effective*" pore space, and the other which consists of non-interconnected or "*isolated*" voids.

In interconnected void space, when the voids are entirely (or partially) filled with water or other fluids, the loading rate should be considered an important factor. When loading rate is low, there is transient flow of the fluid out of the system, and stresses are transferred only in solid structure and not in the fluid. Such conditions are commonly referred to as *drained.* In the same manner, when loading rate is high (which is a typical problem involving bone fractures) there is insufficient time for the dissipation of the excess *pore pressure* generated in the fluid. In this case, called *undrained,* fluid will react against compression forces and will change the stress status in the solid. Generally, these type of materials, which have different behaviour in dry and wet condition, are called *biphasic materials*.

Despite the similarities between porous solids , they exhibit different behavior which depends on many factors including: the type of solid particles, the geometry of void space, etc. The following sections provide a brief review of three typical, yet similar, porous solids (wood- natural; concrete- man-made material and cancellous bone- living organism) in order to demonstrate the different problems involved in the analysis and application of each of these materials.

1.2-wood

In wood, as in other porous solids, properties depend primarily on the porosity and the shape of the cells. If a sample of wood is cut at a sufficient distance from the center of the tree, such that the curvature of the growth ring can be neglected, its properties are orthotropic. It will, subsequently, have three orthogonal planes of symmetry: the radial, the tangential and the axial. The stiffness and strength are greatest in the axial direction; that is, parallel to the trunk of the tree. In the radial and tangential direction they are reduced by a factor of 1/2 to1/20, depending on the species(Gibson,1988). Fig (1.2) shows three orthogonal sections of cedar.

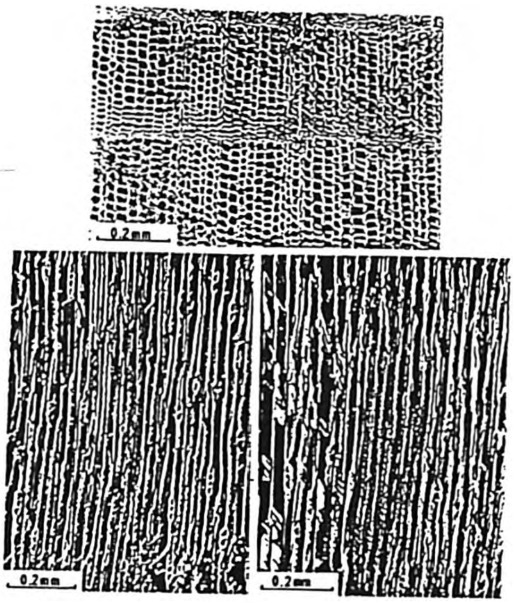

Fig.(1.2)

Three orthogonal section of cedar (from: Gibson,1988)

On a finer scale, that of microns, wood is a fibre-reinforced composite. The lay-up of the cellulose fibers in the wall is complicated but important because it accounts for part of anisotropy of wood; i.e. the difference in properties along and across the grain. It is helpful, though a simplification, to think of the cell walls as a helically shaped wound, with the fiber direction nearer the cell axis rather than across it. This gives the cell wall a modulus and a strength, which are large parallel to the axis of the cell, and smaller , by a factor of about 3, across it. But this accounts for only a portion of the anisotropy of wood. The rest is related to cell shape: elongated cells are stiffer and stronger when loaded along the long axis of the cell than when loaded across it.

The strength of wood is affected by age and moisture content, as well as the temperature and strain rate at which testing is carried out. The general observations from a typical uniaxial compression test, are as follows (Gibson,1988) . At small strain (less than 0.02) the behavior is linear-elastic in all three directions. Young's modulus in the axial direction is much larger than in tangential and radial direction, which are roughly equal. Beyond the linear-elastic regime, the stress-strain curves for loading in all three directions show a stress plateau extending to strain between 0.2 and 0.8 depending on the density of the wood. At the end of the plateau the stress rises steeply. The mechanism of wood fracture, either in static or impact bending, is complicated. Many mechanical models have been developed and suggested for different types of wood and cell structures.

1.3-Concrete

The pore microstructure of concrete has received a great deal of attention in recent years. According to studies (Dullien,1979) the structure of concrete consists of clinker grains that are separated from each other by a hydrated mass of calcium hydrosilicates; in the central portion of which there are thin veins of capillaries which form an interconnected network, as shown schematically in Fig (1.3). The porosities in fine concrete range from 6% to 10%. The pore walls are made up of dense rays of needles which intermesh when calcium chloride has been added to the paste. The hardening time and conditions, composition of cement, water-cement ratio, chemical additives and the type of compacting all play a role in the pore structures of concrete.

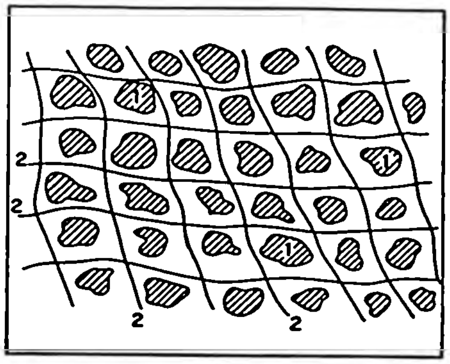

Fig.(1.3)

Schematic picture of a concrete structure: 1) impermeable 2) permeable components

(From: Dullien, 1979)

According to Jung (1973), the formation of pore systems by hydration in concrete follows a specific law which makes it possible to calculate the porosity of hydrated cement and concrete. Other studies (e.g. Romer, 1973) have proposed a microscopic method to differentiate all pore and void spaces in concrete from solids by saturating the sample with liquid polymer, which contains a fluorescent tracer. The samples are then viewed in ultraviolet light.

Most of the theoretical studies on fracture mechanism are based on continuum mechanics theory and refer to homogeneous material while ignoring the presence of the heterogeneous microstructure of the solid. Concrete materials, however, are extremely heterogeneous and include not only flaws but various kinds of structural defects. Up until now only isolated attempts have been made to consider such effects.

1.4-Cancellous bone

Although structural bones appears fairly solid, they actually resemble an elaborate sandwich, made up of an outer shell of dense compact bone enclosing a core of porous cancellous bone. Examples shown in the Fig.(1.4) include cross section of a femur, a tibia, and a vertebra.

In some instances, for example at joints between vertebrae or at the ends of the long bones, this configuration minimizes the weight of the bone while providing a large bearing area , a design which reduces the bearing stresses at joints. In others, as the vault of the skull, it forms a low weight sandwich shell. In either case, the presence of cancellous bone reduces the weight while still meeting its primary mechanical function.

An understanding of the mechanical behavior of cancellous bone has relevance to several biomedical applications. In elderly patients with *osteoporosis* the mass of bone in the body decreases over time to such an extent that fractures can occur under loads that, in healthy people, would have no effect. Such fractures are common in the vertebrae, hip and wrist and are due, in part, to a reduction in the amount of cancellous bone in these areas.The degree of bone loss in a patient can be measured using non-invasive techniques. An understanding of the relationship between bone porosity and strength helps predict when the risk of fracture is high. It also helps in the design of artificial hips. Since most of the bone replaced by an artificial hip is cancellous, an improved understanding of the structure

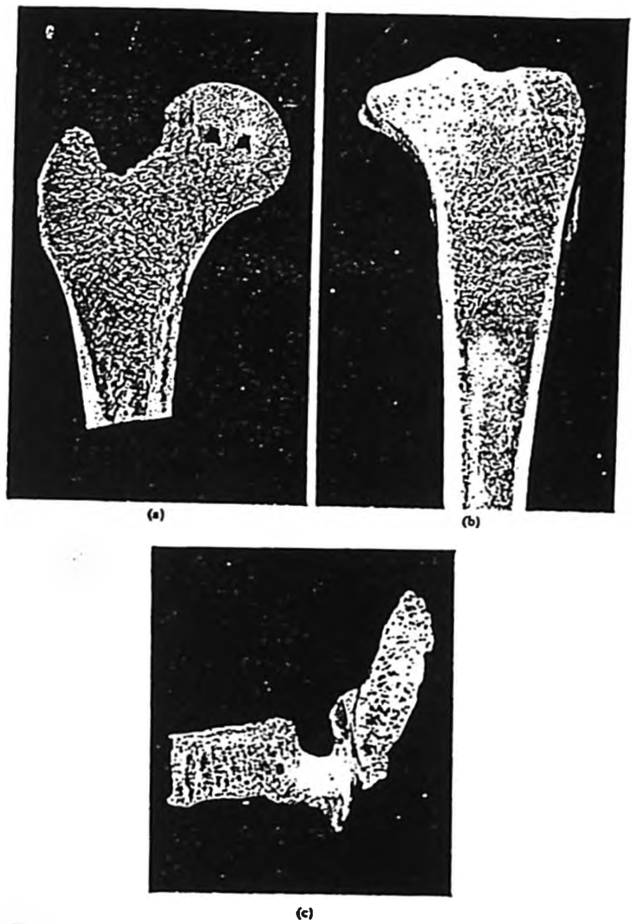

Fig.(1.4)

Cross-section view of a) the head of femur b) the tibia and c) a lumbar vertebra

(From: Gibson, 1988)

property relationships for cancellous bone allows for the design of artificial hips with properties that more closely match those of the bone they replace. The mismatch of properties between current artificial hips and the surrounding bone is a possible explanation for the fact that the fit becomes increasingly loose with time.

The distribution of forces acting across a joint is directly related to the mechanical properties of underlying cancellous bone, so that changes in its structure may affect the distribution of forces and cause damage. The cellular structure of cancellous bone is shown in Fig (1.5). It consists of an interconnected network of rods or plates. A network of rods produces low-density, open cells, while one of the plates gives higher-density,virtually closed cells. In practice, the relative density of cancellous bone varies from 0.05 to 0.7 (technically, any bone with a relative density less than 0.7 is classified as "cancellous"). More details about bone properties will be provided in following chapters.

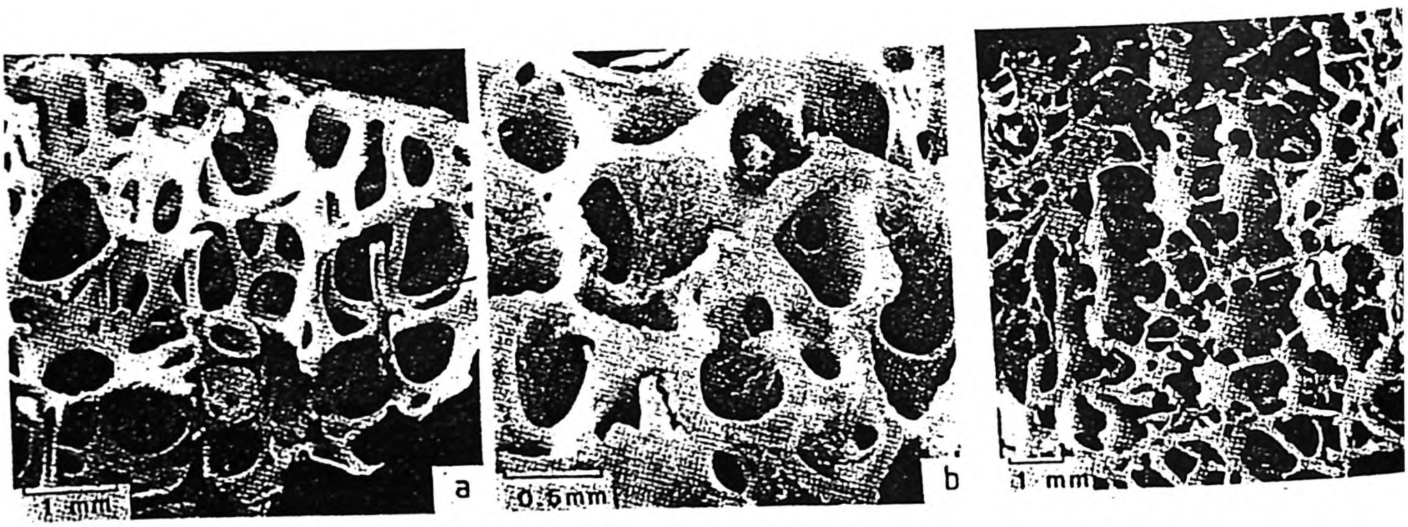

Fig.(1.5)

Specimens taken from a) the femoral head, showing a low density b) femoral head, showing a higher density c) the femoral condyle, of intermediate density

(From: Gibson,1988)

1.5-scope of this project

The main purpose of this project is to analyze the mechanical behavior of porous solids using a modern approach based on continuum mechanics. The formulation of the problem, applications and results are discussed in different chapters.

In chapter 2, the mathematical formulation for describing the mechanics of porous solids is reviewed. Beginning with a short overview of the notion of fabric tensors, this chapter provides a comprehensive discussion on specification of failure criteria for porous solids. Finally, the anisotropic elastic properties of porous solids are investigated.

In chapter 3, the problem of fracture of a femur due to the lateral fall is defined. This particular problem has been selected to demonstrate the applicability of the formulation outlined in chapter 2. First, a short review of the anatomy of the femur is provided followed by an investigation of fracture in the proximal part of the femur. Previous studies are examined and a brief outline of the current research is given.

The results of numerical simulations are given in chapter 4. First, the CT method used to define the geometry and physical properties of femur is reviewed. Then, the details of static analysis are given followed by the presentation of numerical results. The dynamic analysis is investigated next. First, a short review of finite element theories in analysis of propagation problems is given, then the details of the results of dynamic analysis are presented.

In chapter 5, a summary of the project is given, followed by the main conclusions obtained from the results of analyses. Later, some suggestion and recommendation for future research are made.

CHAPTER 2

MATHEMATICAL FORMULATION OF MECHANICAL BEHAVIOR OF POROUS SOLIDS

2.1-INTRODUCTION

The mechanical properties of porous solids depend on porosity, which is a primary factor affecting the material characteristics. At the same time, other parameters, known as fabric tensors, have been used by several researchers (e.g. Cowin,1978). Fabric tensors are commonly employed to describe the orientation of material's microstructure and, further, to define constitutive equation and the corresponding failure criteria.

This chapter provides a brief review of the notion of fabric tensors including a definition and a history of its implementation in the study of different types of porous materials. First, various methods used to calculate fabric tensor are investigated. Following that, the concept of directional porosity is outlined and conditions at failure are discussed. Subsequently the effect of liquid on the mechanical behavior of biphasic materials is investigated and the corresponding constitutive equations are developed. Finally, a brief review of a model, used to define the anisotropic elastic properties of porous solids, is given.

2.2-FABRIC TENSOR

It is commonly recognized that porosity or solid volume fraction affects the mechanical properties in porous materials. At the same time, the properties also depend on the orientation of the principal directions of microstructure in relation to those of the stress state .There appears to be a general agreement that a second rank tensor can be used to describe the orientation of material's microstructure, Cowin (1978). Following the work of Oda (1976), these second rank tensors are generally called *fabric tensors*.

The precise definition of a fabric tensor varies with the type of material and, sometimes for the same material, with the investigator. In general, the fabric tensor is a symmetric second rank tensor which characterizes the arrangement of the microstructural components in a multiphase or porous material. The concept of a fabric tensor applies to any phase of a distributed, multiphase mixture.

In the literature on granular materials and soil mechanics, fabric tensors are considered by Satake (1985,1982), Oda (1976), Oda et al.(1982), Oda et al. (1985), Kanatani (1983) and others. In the literature on rock mechanics, the fabric tensor is employed by Oda (1984), Oda et al. (1984) and others. In the literature on cancellous or spongy bone mechanics, the concept of fabric tensor was introduced by Harrigan and Mann (1984) and employed by Cowin (1986).

The general problem of the quantification of structural anisotropy in materials with distinctive microstructures, such as geological and biological materials, was examined in a series of papers by Kanatani (1984a, 1984b, 1985a, 1985b). The problem of the determination of structural anisotropy by methods of quantitative stereology was first considered by Hillard(1967). Kanatani expanded the distribution density function in spherical harmonics and obtained an infinite series of even rank tensors. The definition of fabric tensors given by Kanatani is relatively universal and specific. The actual definition to be used in any particular situation is clearly material dependent. The following is a brief review of some of the theories related to the notion of fabric tensors.

A) The Mean Intercept Length Method;

Whitehouse (1974) and Raux et al.(1975) provided the first detailed description of cancellous bone architectural anisotropy using an intersection counting technique. Raux et al. expressed the results as *roses of orientation* (1970), whereas, Whitehouse took results one step further and expressed the results by the mean intercept length (MIL) measure. The principle of the MIL method is to count the number of intersections between a linear grid and the bone marrow interface as a function of the grid's orientation, ω ; see Fig.(2.1).

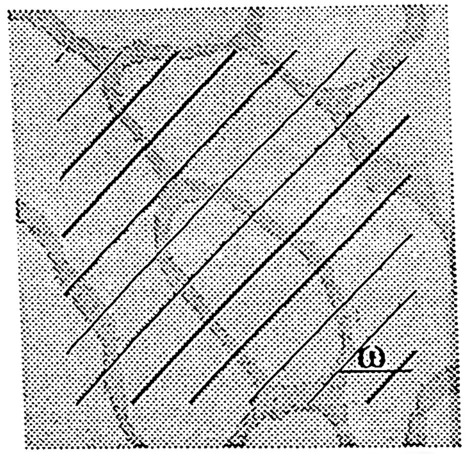

Fig.(2.1)

(From: Odgaard,1997)

The mean intercept length (the mean length between two intersections) is simply the total line length divided by the number of intersections:

$$MIL(\omega) = \frac{L}{I(\omega)} \tag{2.1}$$

Whitehouse (1974) defined the mean intercept length in bone (MIL_b) and marrow (MIL_m) as

$$MIL_p = 2V_v MIL(\omega) \tag{2.2}$$

where p is the phase of interest (bone or marrow) and V_v is the volume fraction. The reason for factor 2 is that 2MIL is the mean length of a bone + marrow intercept. Multiplying MIL by a constant, as in equation (2.2), does not change the anisotropy information. The equation (2.2) has been used by some investigators, such as Synder et al.(1989), Kuhn et al.(1990) and Goulet et al.(1994). Their argument for doing so is that the absolute size of intercept length (or pore size) may have significance in architecture-mechanics relations. There are, however, empirical and theoretical arguments for disregarding pore size. Many investigators, including Wang (1984) ,Turner et al. (1987) and Gibson et al.(1988) believe that the benefits of using the equation (2.2) have yet to be proven.

Whitehouse observed that 2-D MIL results, when plotted in a polar diagram, generate an ellipse, and the parameter of this ellipse would thus provide a convenient way of describing anisotropy. These 2-D observations may be generalized to 3-D space, where a polar plot of quantifying MIL data is assumed to approximate an ellipsoid, and an ellipsoid may be expressed by the quadratic form of a second rank tensor known as the MIL fabric tensor.

When 3-D reconstructions are available, it is possible to determine the MIL data directly in 3-D space. Methods for determining the MIL fabric tensor from perpendicular 2-D sections have been described by Harrigan et al.(1984) and Kanatani(1985). Hodgskinson and Currey (1990) determined MIL ellipses on the four faces parallel to the loading orientation on the cancellous bone cubes and defined a combined expression for MIL fabric tensor. A similar approach was taken by Harrigan et al.(1981).

B)The Volume -Based Methods

Because MIL is unable to detect some forms of architectural anisotropy, volume-based measures were introduced, including the volume orientation (VO) method proposed by Odgaard et al.(1990). The results incorporating volume-based measures may also be expressed in terms of positive definite, second rank tensors. In general the volume-based methods shift the interest of architectural anisotropy from interface to volume.

B1-Volume orientation

A local volume orientation is defined for any point within a trabecula as the orientation of the longest intercept through the point (See Figure 2.2).

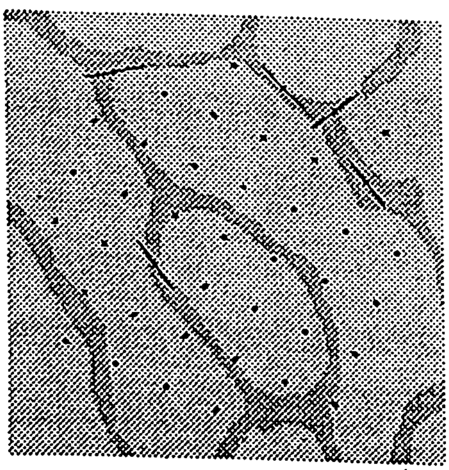

Fig.(2.2)
(From: Odgaard,1997)

The local volume orientation, ω , has a semicircular orientation in 2-D space, a hemispherical orientation in 3-D space, and it is assumed that ω is uniquely defined for any point within the bone. The result for volume orientation (VO) measurements may be expressed by a VO fabric tensor, which describes the typical distribution of trabecular bone volume around a common point within a trabecula. This is in contrast to the MIL fabric tensor, which describes the orientation of interfaces between bone and marrow.

In the original description of the VO method, a technique for inferring a concentration parameter, κ from the individual 2-D section was developed. There are three prerequisites for using this technique. First, a parametric distribution function must be assumed; second , a geometric model for the trabecular architecture must be assumed; and third, the main orientation of the volume orientation distribution must be known. All these assumptions are critical and require substantial documentation, with true 3-D measurements being preferred.

Basic properties of the VO method have been examined by Odgard et al.(1997). For rectangular particles, the VO method results in blurring around diagonal orientations. However, it should be kept in mind that the VO method was not developed for particle systems.

B2-star volume and star length distribution

The star volume distribution (SVD), like the volume orientation method, describes the distribution of trabecular bone around a typical point in a trabecula (see Figure 2.3). The star volume distribution is closely related to star volume measure. The star length distribution provides a minor modification of the SVD measure. The results of SVD (or SDL) measurement may also be expressed by a normalised fabric tensor ,the SVD *fabric tensor.* Fig.(2.3).

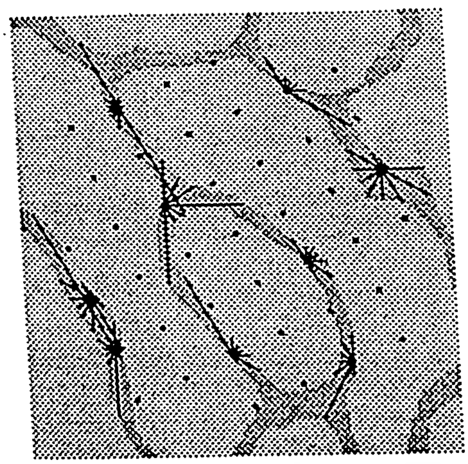

Fig.(2.3)

(From: odgaard,1997)

C)Directional Porosity Method;

In this section the concept of directional porosity, presented by Pietruszczak et al.(1995) is briefly reviewed. Directional porosity is used as an implicit measure of the internal structure of materials and could be recognized as the generalized ,direction-dependent counterpart of"porosity"(i.e. the scalar valued quantity defining void space fraction). The directional porosity is constructed as an average, continuous and non-singular measure in the form of an integral over a representative volume. It is also mathematically expressed in the form of generalized Fourier series (Pietruszczak et al,1988). Its values can be estimated directly from experiment by means of quantitative microscopy and, in particular, by the lineal analysis.

In order to construct a directional measure of voids distribution, consider a sphere (S) of a unit radius R=1, which encloses a representative volume of the material. See Figure(2.4).

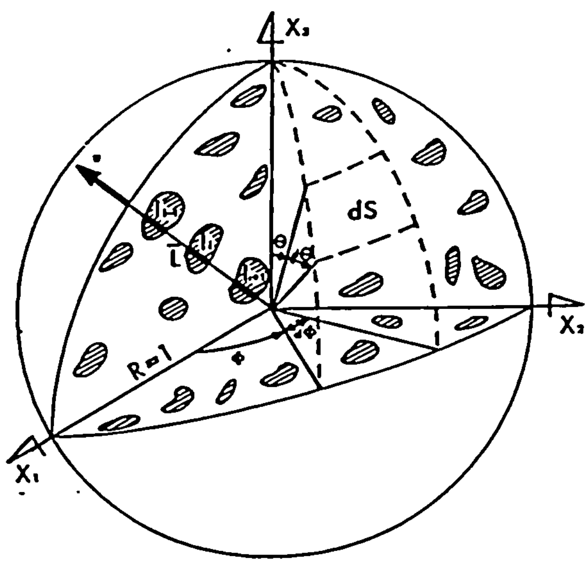

Fig.(2.4)

Unit sphere enclosing a representative volume of material
(From: Pietruszczak, 1995)

Next, consider a test line of length $\bar{L} = 2R$ with the orientation ν_i with respect to the fixed Cartesian coordinate system. The fraction $\bar{L}$ occupied by voids can be defined as

$$L(\nu_i) = l(\nu_i) / \bar{L}; \qquad l(\nu_i) = \sum_k l_k(\nu_i) \tag{2.3}$$

where $l(\nu_i)$ represents the total length of interceptions of this line with the void space. The mean value of the quantity $L(\nu_i)$, averaged over the domain S, is

$$L_{av} = \frac{1}{4\pi}\int_s L(\nu_i) f(\nu_i) dS \quad ; \quad \frac{1}{4\pi}\int_S f(\nu_i) dS = 1 \tag{2.4}$$

where $f(\nu_i)$ is a scalar valued function describing the spatial distribution of test lines. It can be shown that, for uniformly distributed test lines, the first integral in the above equation is the measure of average porosity of the material, n , whereas the lineal fraction occupied by pores is an unbiased estimator of the volume fraction of voids in the direction ν_i, i.e.

$$n = L_{av} \quad ; \quad \bar{n}(\nu_i) \equiv L(\nu_i) \tag{2.5}$$

The scalar valued function $\bar{n}(\nu_i)$, defined over the unit sphere S can be represented by the generalized double Fourier series. The desired best fit approximation can be established by the 'least square' method. This leads to a representation in terms of symmetric traceless tensors $\Omega_{ij}, \Omega_{ijkl}, ...$(cf.Kanatani, 1984).

$$\bar{n}(v_i) = n(1 + \Omega_{ij} v_i v_j + \Omega_{ijkl} v_i v_j v_k v_l + ...) \tag{2.6}$$

The higher rank of tensors Ω_{ijkl}, ... relate to the higher order fluctuations in void space distribution. Thus, in order to describe a smooth orthogonal anisotropy, it is sufficient to employ an approximation based on the first two terms of the expansion (2.6) . Consequently, the function may be defined as:

$$\bar{n}(v_i) \approx 3nA_{ij} v_i v_j \quad ; \qquad A_{ij} = \frac{1}{3}(\delta_{ij} + \Omega_{ij}) \Rightarrow A_{ii} = 1 \tag{2.7}$$

where A_{ij} is referred to as the fabric tensor.

2.3-FAILURE CRITERIA

In recent studies by Pietruszczak et al.(1999a), a new criterion for fracture of anisotropic porous materials has been proposed. The general method in the formulation of failure criteria for anisotropic materials, which includes proper tensor generators and invariants, is mathematically complex and requires extensive experimental data for identification of material parameters. To solve this problem, a simpler approach is used. In the proposed fracture criterion, a scalar-valued function defining the 'directional porosity' is employed, which is perceived as a measure of material fabric. This measure, as previously explained, describes the spatial distribution of void fraction in the neighbourhood of the material point and it is identifiable from 3D micro-computed tomography. This approach is general enough to allow for the implementation of different orientation-dependent parameters describing the material architecture.

The basic idea underlying the fracture criterion is that there exists a function F of the stress state σ_{ij} and the fabric A_{ij} such that if the ultimate state of the material is reached, the value of this function is constant.(i.e zero)

$$F(\sigma_{ij}, A_{ij}, n) = 0 \tag{2.8}$$

Since the anisotropy of fabric is fully described by A_{ij}, F must be an isotropic function of both σ_{ij} and A_{ij}

$$F(\sigma_{ij}, A_{ij}, n) = F(T_{ip} T_{jq} \sigma_{pq},\ T_{ip} T_{jq} A_{pq}, n) \tag{2.9}$$

where T_{ij} represents the transformation tensor. A general form of F may be obtained by expanding this function in a polynomial in the components of σ_{ij}. Cowin (1986) has developed a simple quadratic approximation

$$F = G_{ij}\sigma_{ij} + B_{ijkl}\sigma_{ij}\sigma_{kl} = const. \tag{2.10}$$

where

$$\begin{aligned} G_{ij} &= g_1\delta_{ij} + g_2 A_{ij} + g_3 A_{im}A_{mj} \\ B_{ijkl} &= f_1\delta_{ij}\delta_{kl} + f_2(A_{ij}\delta_{kl} + \delta_{ij}A_{kl}) + f_3(\delta_{ij}A_{kq}A_{ql} + \delta_{kl}A_{iq}A_{qj}) + f_4 A_{ij}A_{kl} + \\ &\quad f_5(A_{ij}A_{kq}A_{ql} + A_{is}A_{sj}A_{kl}) + f_6 A_{is}A_{sj}A_{kq}A_{ql} + f_7(\delta_{ki}\delta_{lj} + \delta_{li}\delta_{kj}) + f_8(A_{ik} \\ &\quad A_{il}\delta_{kj} + A_{lj}\delta_{ki}) + f_9(A_{ir}A_{rk}\delta_{lj} + A_{kr}A_{rj}\delta_{li} + A_{ir}A_{rl}\delta_{kj} + A_{lr}A_{rj}\delta_{ik}) \end{aligned}$$

and g's and f's are scalar valued functions of the basic invariants of A_{ij} and the average porosity.

There are some difficulties associated with the above approximation. First, it requires an extensive experimental program to identify the twelve functions of the material fabric. Second, it is obvious that the behaviour of porous material depends on the third stress invariant(Desai et al.1987). Hence, this approximation as well as other commonly used criteria (e.g., Tsai and Wu, 1971), can not completely describe the conditions at failure.

In order to overcome this problem, an alternative to representation (2.8) is employed, following a general approach proposed by Pietruszczak (1999b). In particular, it is postulated that the functional form of the fracture criterion incorporates directly $\bar{n}(\nu_i)$, so that

$$F = F\left(\sigma_{ij},\ \bar{n}(l_i)\right) = 0 \tag{2.11}$$

Here, the function $\bar{n}$ is evaluated in the 'loading direction' l_i, which can be defined here as the direction of the average stress vector T_i at a point, i.e.

$$T_i = \sigma_{ij}(e_j^{(1)} + e_j^{(2)} + e_j^{(3)}) = \sqrt{3}\,\sigma_{ij}m_j \tag{2.12}$$

$$l_i = \frac{T_i}{\|T_i\|} = \frac{\sigma_{ij}m_j}{(\sigma_{kl}\sigma_{kp}m_l m_p)^{1/2}} \tag{2.13}$$

where e_i's are the base vectors associated with the principal material axes and $m_i=\{1,1,1\}/\surd 3$ is a unit vector along the space diagonal. Since (2.11) must be an isotropic function of stress,

$$F\left(\sigma_{ij},\ \bar{n}(l_i)\right) = F\left(T_{ip}T_{jq}\sigma_{pq},\ \bar{n}(T_{ip}l_p)\right) = F\left(I_1, I_2, I_3,\ \bar{n}(l_i)\right) = 0 \tag{2.14}$$

where I's are the basic invariants of σ_{ij}. Alternatively, F may incorporate any convenient measures which are derived from the basic invariants. A general form of representation (2.14), pursued further, is

$$F = F\left(I, \bar{\sigma}, \theta,\ \kappa_n(l_i)\right) = 0 \tag{2.15}$$

where $I=-\sigma_{ii}$, $\bar{\sigma}=(\frac{1}{2}\, s_{ij}s_{ij})^{\frac{1}{2}}$, $\theta=1/3\,\sin^{-1}\{(\surd 3\; s_{ij}s_{jk}s_{ki})/2\bar{\sigma}^3\}$ and s_{ij} represents the stress deviator. In Eq.(2.15), κ_n (n=1,2,...,N) represents a set of material parameters embedded in a typical formulation describing an isotropic response whereas the invariants (I, $\bar{\sigma}$, θ) are chosen to provide a simple geometric interpretation of the fracture criterion.

It seems rational to adopt a functional form typically employed for brittle-plastic materials. One particular formulation, describing an *isotropic* material, is that proposed by Pietruszczak et al. (1988), viz.,

$$F = a_1\left(\frac{\bar{\sigma}}{g(\theta)f_c}\right) + a_2\left(\frac{\bar{\sigma}}{g(\theta)f_c}\right)^2 - \left(a_3 + \frac{I}{f_c}\right) = 0 \qquad (2.16)$$

Or equivalently,

$$F = \bar{\sigma} - g(\theta)\,\bar{\sigma}_c = 0; \qquad \bar{\sigma}_c = \frac{-a_1 + \sqrt{(a_1^2 + 4a_2(a_3 + I/f_c))}}{2a_2} f_c \qquad (2.17)$$

where the parameters a_1, a_2, a_3 are dimensionless material constants and f_c represents the uniaxial compressive strength. Moreover, the function $g(\theta)$ is selected in the form:

$$g(\theta) = \frac{\left(\sqrt{(1+a)} - \sqrt{(1-a)}\right)K}{K\sqrt{(1+a)} - \sqrt{(1-a)} + (1-K)\sqrt{(1-a\sin 3\theta)}}; \qquad a = const. \qquad (2.18)$$

which satisfies $g(\pi/6)$=1 and $g(-\pi/6)$=K and for a=0.999 guarantees convexity for $K \geq 0.565$. It should be noted that according to Eq.(2.17), K is a material parameter which represents the ratio of the maximum deviatoric stress intensity $\bar{\sigma}$ in compression ($\theta = \pi/6$) and extension ($\theta = -\pi/6$) domains for a fixed value of I=const.

In general, the material parameters a_1, a_2, a_3 can be identified from standard material tests (i.e. uniaxial compression/tension and biaxial compression). The details on the identification procedure are provided by Pietruszczak et al. (1988). Typically, the strengths in uniaxial tension and biaxial compression are proportional to f_c, so that f_c may be considered as the only independent parameter.

The simplest extension of Eqs.(2.16) and (2.17) to *anisotropic* conditions, consistent with representation (2.15), is that in which a's are assumed to remain constant and $f_c = f_c(l_i)$,

$$f_c(l_i) = f_{co}\left(\frac{\rho}{\rho_o}\right)^{\gamma} = f_{co}\left(\frac{1-\bar{n}(l_i)}{1-n_o}\right)^{\gamma} \tag{2.19}$$

Here, ρ is the density of the bone material (considered as orientation-dependent) and γ is a constant, typically within the range $1 \le \gamma \le 2$ (Keller, 1994). In the principal stress space, Eqs. (2.16) and (2.17) represent an irregular cone with smooth curved meridians and a non-circular convex cross-section in the deviatoric (π) plane (Fig.2.5). The shape of the π-plane section is defined through the function $g(\theta)$, Eq.(2.18).

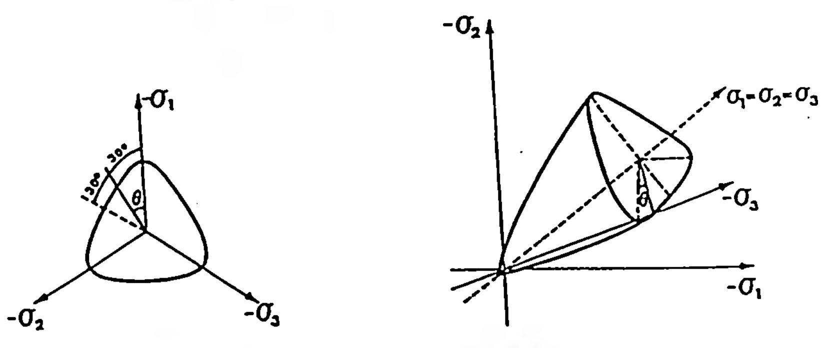

Fig.(2.5)

Failure surface in principal stress space (for $f_c = const.$)

(From : Pietruszczak, 1995)

In general, Eqs.(2.16) and (2.17) together with Eq.(2.19) define the fracture criterion for cortical as well as trabecular bone. In a phenomenological sense, both these tissues are considered here to be the same material with different porosity characteristics, Eq.(2.8), which affect the strength viz. Eq.(2.19).

2.4-Failure criteria in biphasic materials

Introduction

The presence of liquid in a porous solid can influence the mechanical properties in two different ways. Firstly, it may affect them by chemical alteration. Secondly, when the material is in compression the deformation process is constrained and the behaviour is different from that observed in the dry material. Terzaghi's effective stress principle, which is typically employed in soil mechanics, has also been extensively used for saturated porous solids. In addition, it has been used in rock mechanics, by Stagg et al.(1968), Goodman(1980) and Brady et al.(1985), as well as for problems involving concrete structures by Zienkiewicz et al.(1989) and Zienkiewicz(1991). According to this principle, total stress is decomposed into two parts. The first part deals with the solid phase and is called effective stress while the other part represents the excess of pore water pressure. It is assumed that the deformation process and failure criteria are governed by the state of effective stress only. In general, the applicability of Terzaghi's principle in porous solids is questionable. Porous solids are defined as having a continuous matrix of solid phase, which is in contrasts to soils that consist of discrete particles. Furthermore, in soils, the compressibility of water is negligible as compared to that of the skeleton, which is not the case for other porous solids, where the two are of the same order of magnitude.

An accurate description of the mechanical properties of saturated porous solids is considerably important in engineering analysis and design. There are many kinds of engineering structures composed of natural porous solids, which are either partly or completely filled with fluids. Hence, the viability and safety aspect should be taken into account when assessing the two-phase nature of the material. In a study by Pietruszczak and Pande(1995), the authors proposed a constitutive relation governing the undrained behaviour of a porous solid treated as a brittle-plastic material. The formulation is based on a revised stress decomposition, which incorporates an average stress measure in constituents (i.e. solid matrix and liquid). In what followes this formulation is briefly reviewed and later applied in the context of biological materials.

Mathematical Formulation

In saturated porous materials, when the loading rate is sufficiently high, there is not enough time for the dissipation of excess pore pressure generated in the fluid. This case is commonly referred to as undrained, implying that there is no transient flow of the fluid out of the system. To describe the mechanical properties in a biphasic structure, the average macroscopic stress can be defined as (Pietruszczak and Pande,1995):

$$\sigma_{ij} = \frac{1}{V}\left(\int_{V_S} \bar{\sigma}_{ij}^{m}\, dV_S + \int_{V_V} \bar{p}_f\, \delta_{ij} dV_V\right) \tag{2.20}$$

so that

$$\sigma_{ij} = (1-n)\sigma_{ij}^{m} + np_f\delta_{ij} \tag{2.21}$$

In the above formula $\bar{\sigma}_{ij}^{m}$ is the average stress in the solid matrix , p_f is the average excess of the fluid pressure while n represents the average porosity of the material. Eq.(2.24) may also be expressed as:

$$\sigma_{ij} = \sigma_{ij}' + np_f\delta_{ij} \quad ; \qquad \sigma_{ij}' = (1-n)\sigma_{ij}^{m} \tag{2.22}$$

In equation (2.22) σ_{ij}' represents average stress in the solid matrix referred to the unit area of the sample. In the case when the material is elastic and there is no fluid in the system, the mechanical response is defined as:

$$\sigma_{ij} = \sigma_{ij}' = D_{ijkl}\varepsilon_{kl} \quad ; \qquad D_{ijkl} = D_{ijkl}(A_{pq}, n) \tag{2.23}$$

where D_{ijkl} represent the drained elastic properties.

In a biphasic system, a change in pore pressure would trigger a change in the average stress in the solid matrix of a magnitude equal to $\sigma_{ij} = (1-n)p_f\delta_{ij}$. Thus, in order to maintain consistency with the characteristics for dry materials, equation (2.23) must be revised to

$$(\sigma'_{ij} - (1-n)p_f\delta_{ij}) = D_{ijkl}\varepsilon_{kl} \tag{2.24}$$

The above equation can now be combined with the constitutive relation for the pore fluid. Neglecting the viscous effects and assuming that the fluid is linearly compressible:

$$p_f = K_f\varepsilon^f_{ii} \quad ; \qquad \varepsilon^f_{ii} = \varepsilon_{ii} / n \tag{2.25}$$

where K_f represents the bulk modulus of the fluid. Generally, the volume change of material is caused by the change in the volume of voids. When voids are connected and filled with a fluid, the total deformation must be consistent with that of the fluid itself. Hence, the combination of equation (2.24) and (2.25) would result in:

$$\sigma'_{ij} = (D_{ijkl} + (1-n)C_{ijkl})\varepsilon_{kl} \; ; \qquad C_{ijkl} = \frac{K_f}{n}\delta_{ij}\delta_{kl} \tag{2.26}$$

or, in view of equation (2.22)

$$\sigma_{ij} = (D_{ijkl} + C_{ijkl})\varepsilon_{kl} \tag{2.27}$$

The above equation represents the constitutive relation for a porous solid considered as an elastic biphasic system. For these type of materials, the failure criterion can be expressed as;

$$F = F(\sigma'_{ij}, n(l_i)) = 0 \tag{2.28}$$

where σ'_{ij} is the average stress in the solid skeleton.

2.5-Anisotropic elasticity of porous solids

In porous solids, such as bone, mechanical properties are closely related to the microstructure . As previously discussed, the microstructural properties associated with pore distribution can be described using a set of fabric tensors which can be identified by means stereological methods (Kanatani,1984). Integral geometry or stereology is a body of mathematical methods for estimating 3D morphological parameters from 2D or 1D projections (Weibel,1980).

An elementary microstructural description is contained in a single scalar property such as relative density, while material anisotropy requires a fabric tensor of a higher rank. However, in many applications, microstructure anisotropy seems to be sufficiently well described by a scalar and symmetric, traceless second rank fabric tensor, which restricts material symmetry to orthotropy.

In solid materials, linear elastic properties are characterized by one fourth rank tensor (Curnier et al.,1995). One of the attempts to relate a fabric tensor to a fourth rank elasticity tensor can be found in Cowin(1985). He suggested a model based on a normalized second rank tensor and reported expression for the elastic constants in terms of the invariants of fabric tensors.

Another attempt can be found in the study by Zysset et al. (1996), where a general approach for relating the material microstructure to the fourth rank elasticity tensor has been proposed. In this approach, an approximation based on the Fourier series decomposition has been employed. Following this concept, the orthotropic elastic moduli are defined as:

$$E_i = E_o[\rho_s(1-n)]^2 A_i^{-2} \qquad \text{(i,j=1,2,3 and i<j)} \qquad (2.29)$$

$$G_{ij} = G_o[\rho_s(1-n)]^2 A_i^{-1} A_j^{-1} \qquad (2.30)$$

$$\mu_{ij} = \mu_o \frac{A_i}{A_j} \qquad (2.31)$$

subject to the constraint $\mu_o = E_o/(2G_o) - 1$. In the above equations, E's are Young's moduli, G's are shear moduli, μ represents Poisson ratios. A's are the eigenvalues of the fabric tensor, ρ_s is density , n is average porosity and E_o, G_o, μ_o are material constants. The compliance tensor in the principle orientation of the fabric tensor exhibits the form:

$$D = \begin{bmatrix} \frac{R_C}{A_1^2} & \frac{Q_C}{A_1A_2} & \frac{Q_C}{A_1A_3} & 0 & 0 & 0 \\ \frac{Q_C}{A_1A_2} & \frac{R_C}{A_2^2} & \frac{Q_C}{A_2A_3} & 0 & 0 & 0 \\ \frac{Q_C}{A_1A_3} & \frac{Q_C}{A_2A_3} & \frac{R_C}{A_3^2} & 0 & 0 & 0 \\ 0 & 0 & 0 & \frac{G_C}{A_1A_2} & 0 & 0 \\ 0 & 0 & 0 & 0 & \frac{G_C}{A_2A_3} & 0 \\ 0 & 0 & 0 & 0 & 0 & \frac{G_C}{A_1A_3} \end{bmatrix} \qquad (2.32)$$

Where,

$$Q_C = \frac{E_o\mu_o[\rho_s(1-n)]^2}{(1+\mu_o)(1-2\mu_o)}$$

$$R_C = Q_C + 2G_o[\rho_s(1-n)]^2$$

CHAPTER 3

STUDIES OF THE FRACTURE OF THE PROXIMAL FEMUR, A REVIEW

3.1-Introduction

Fractures of the proximal part of the femur are a significant public-health problem as well as a major source of mortality and morbidity among the elderly. In the USA over 260,000 hip fractures occur each year in patients 65 yr of age or older (Graves, 1992). Studies by Bauer (1960), Lewinnek et al.(1980) and Melton et al.(1987) indicate that the incidence of fractures of the hip increases exponentially with age; beginning at about forty years of age for women and forty five years of age for men, and rising at eighty years to an aggregate rate of between 20 and 30 per cent for women and between 10 and 15 per cent for men. Consequently, nearly one out of every three women and one out of every six men could sustain a fracture of the hip by the age of ninety years. This problem is expected to worsen with the projected increase in the average age of the world's population.

In this chapter the femur anatomy along with some of the basic theories of bone mechanics are reviewed. Subsequently, The previous studies on the fracture of proximal femur are examined. Finally, a brief outline of the current research which is an extension of the work of Pietruszczak et al, (1999a), is given.

3.2-Femur anatomy

In this section a brief review of the anatomy of femur is provided. Based on Gray(1995), femur is the longest and strongest bone in human body, see Fig(3.1).

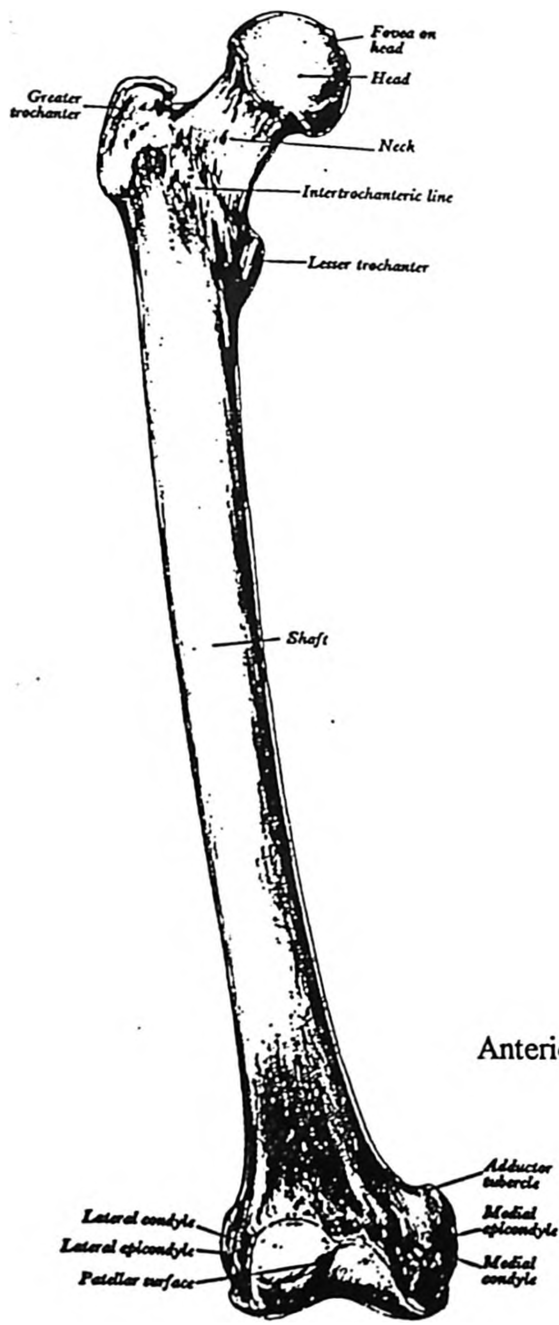

Fig.(3.1)
Anterior aspect of right femur (from: Gray,1995)

Its length is associated with a striding gait, its strength with weight and muscular forces. Its *shaft,* almost cylindrical in most of its length and bowed forward, has a proximal round, *articular head* projecting mainly medially on its short *neck.* In a standing position, the femora are oblique, their heads separated by the pelvic width, their shafts converging downwards and medially to where the knees almost touch. Since the tibia and fibula descend vertically from the knees, the femoral obliquity approximates the feet, bringing them under the line of body weight in standing or walking. The narrowness of this base detracts from stability but facilitates forward movement. Femoral obliquity varies, though it is greater in women due to the relatively greater pelvic breadth and shorter femora. Proximally the femur comprises a head, neck and greater and lesser trochanters.

Proximal end

Slightly more than half a sphere, it faces to articulate with the acetabulum. More precisely, the head is not part of true sphere but rather it is sphenoidale and part of the surface of an ovoid. It's smoothness is interrupted to its center by a small, rough *fovea.* See Fig(3.2).

Femoral neck

About 5 cm long, the femoral neck connects the head to the shaft at an angle of about 125 degrees (*angle of inclination*). This facilitates movement at the hip joints, enabling the limb to swing clear of the pelvis. The neck is also laterally rotated with respect to the shaft (*angle of anteversion*) some 10-15 degrees. There also appears to be some racial variation in anteversion. Narrowest in its midpart and widest laterally, the contours of the neck are rounded; the upper almost horizontal and

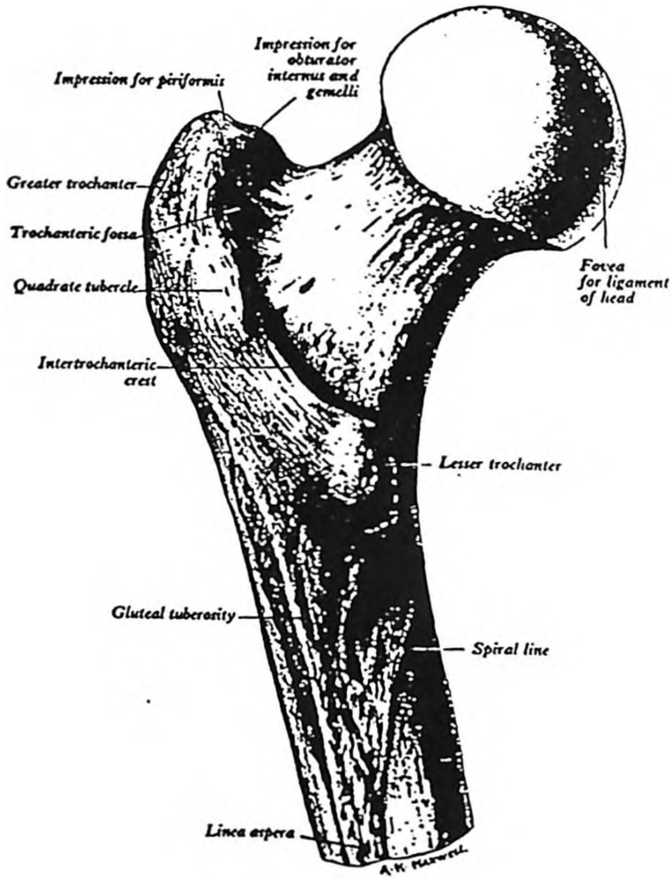

Fig.(3.2)

The proximal part of left femur (from: Gray,1995) slightly concave above, the lower straight but oblique and backwards to the shaft near the lesser trochanter. The neck's anterior surface is flat and marked at the junction with the shaft by a rough *intertrochanteri line*. The posterior surface, facing back and up, is transversel convex and concave in its long axis and it's junction with the shaft is marked by the rounded *intertrochanteric crest*.

3.3- Basic Theories in Bone Mechanics

In biological terms, bone is considered to be a connective tissue. A tissue is an aggregation of similarly specialized cells united in the performance of a particular function. Connective tissue is the tissue which bends together and supports the various structures of the body.

In mechanical terms bone is a composite material with several distinct solid and fluid phases. Bone is unique among the connective tissues because it is hard due to its major organic component being impregnated with a mineral phase, principally hydroxy apatite or very similar crystals. At the macroscopic level there are two major forms of bone tissue: called compact or cortical bone and cancellous or trabecular bone. The location of these bone types in a femur is shown in Fig.(3.3). Cortical or compact bone is a dense material with a specific gravity of about two. The external surface of bone ,which is smooth, is called the periosteal surface. The interior surface is called the endosteal surface. Cancellous bone is also called trabecular bone because it is composed of short struts of bone material called trabeculae. The connected trabeculae

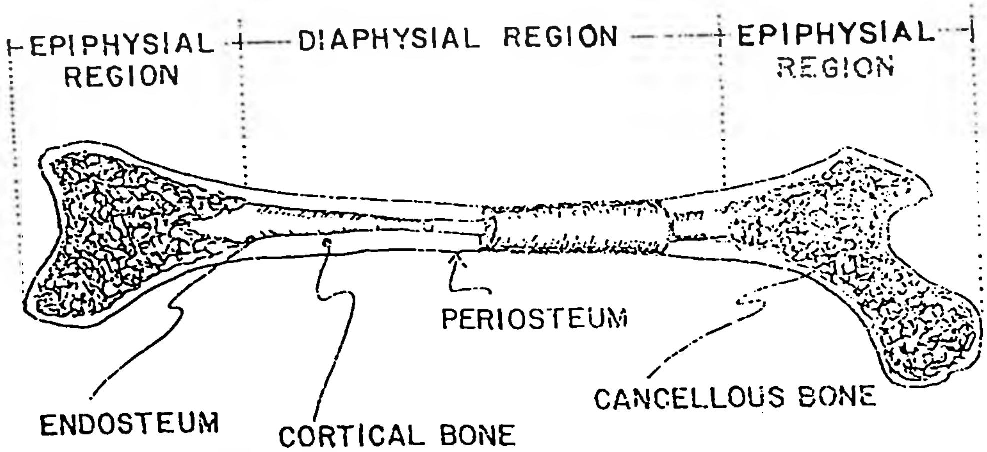

Fig.(3.3)

Longitudinal section of the femur illustrating cancellous and cortical bone type

(From: Cowin, 1981)

give cancellous bone a spongy appearance which is why it is often called *spongy bone*. Though there are no blood vessels within the trabeculae, there are vessels immediately adjacent to the tissue that weave in and out of the large spaces between the individual trabeculae.

Historically the first attempt to explain the structure of cancellous bone on an elastomechanical basis was made by G.H. Meyer in 1867, who published a paper in which he presented a plate with line drawing of cancellous structures he had found in various bones. Culmann in 1867 pointed out that "the line in these drawings very much resembled those curves called the curves of maximum pressure and maximum tension in graphic statics." Meyer (1867) reported that, Culmann asked a student of his to construct the principle stress trajectories in a crane-like curved bar loaded in a fashion similar to the human femur(Fig.3.4). This construction was to become the famous *Culmann crane* and is referred to by many in the publications that followed. The similarity between the idealized structure of cancellous bone in the proximal end of the femur and the trajectories in the Culmann crane, led Meyer(1867) to conclude that the structure of cancellous bone was generally determined by the direction of the principle stresses.

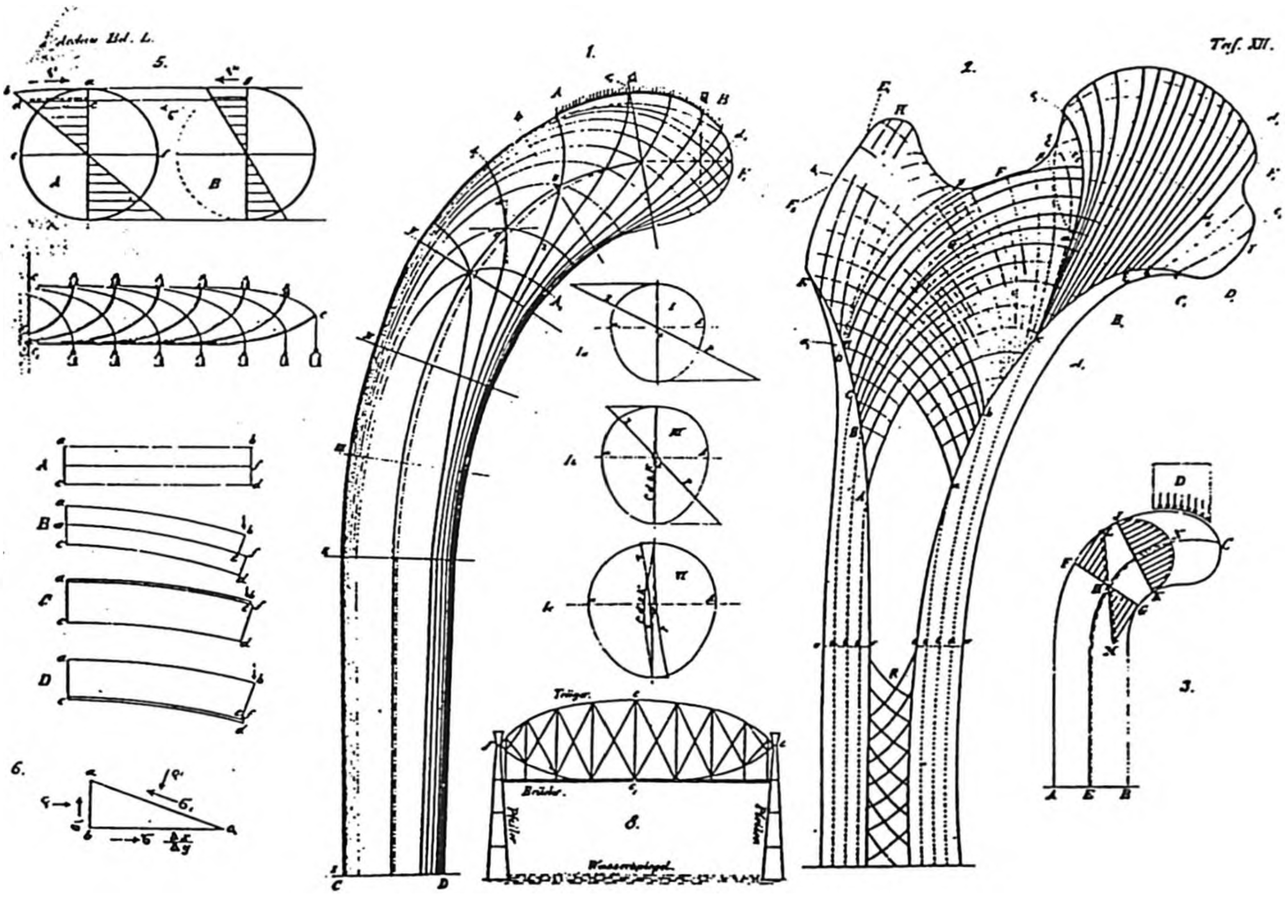

Fig.(3.4)

On the left is Culmann's crane with the principal stress trajectories indicated. On the right is Von Meyers sketch of the trabecular architecture in a section through the proximal end of human femur. Both the femur and culmann's crane are loaded transversely at their cantilevered ends as illustrated on the little insert at the lower far right (from: Cowin, 1986a)

The term “law of bone transformation” was mentioned by Wolff(1892) for the first time based on the assumption that a feedback loop can be described in which the input is a changing loading pattern while the output is an altered bone architecture. Wolff adopted this view in stating:

> “Every change in the form and function of a bone or of their function alone is followed by certain definite changes in their internal architecture, and equally definite secondary alteration in their external conformation, in accordance with mathematical laws.”

Roux (1895) proposed a “trajectorial architecture” to describe the geometry of trabecular bone and to explain how it is organized to provide maximum strength with a minimum amount of material. According to Murray (1936), the fundamental idea in the trajectorial theory is that trabeculae follow the stress trajectories in the homogenous body of the same form. Pauwels (1948) conducted photoelastic experiments directed toward this theory while Kummer (1966) demonstrated, qualitatively, the similarity between a three-dimensional trajectorial model of the femur and the trabeculae architecture.

There has been a lively debate in the orthopaedic and anatomic literature on the mechanical factors controlling the architecture of trabecular bone (i.e.Tobin,1968,Oxnard,1972, Takechi,1977). More recent stress analyses of the proximal femur, based largely on the finite element method, have tended to support the trajectorial theory.Clinical interest has also focused on change in the trabecular architecture of the proximal femur as an index of osteoporosis (i.e. Jowsey,1977).

Historically a number of papers have dealt primarily with cortical bone. Frost (1964) suggested that bone form may change in response to intermittent surface strain, supporting the theory that bone drifts toward the load-induced concavity, thereby neutralizing bending and putting the whole bone in compression. Lanyon (1974) also showed that in the sheep cancellous bone, the trabeculae are aligned approximately along principle strain directions. Later in 1976, Lanyon suggested that this alignment may be advantageous for reducing shear strain.

For trabecular bone, Radin (1972) and Pugh et al.(1974) proposed a damage accumulation hypothesis based on Wolff's law and suggested a central role for trabecular microstructures in various stages of healing in trabecular bone in both human and rabbits. It was also demonstrated that healing increases the mass and stiffness of trabeculae.

In recent years, there has been an increased research interest in trajectorial theory of bone architecture. This increased research interest is driven by two major factors. First, there is the clinical need to understand the mechanical behavior of bone tissue due to the use of implanted bone which has increased significantly. Second, scientific and experimental techniques developed in the field of physical and biological science as well as in the field of engineering now supply the technology that, in the past, blocked further development.

3.4- A review of studies on fracture of proximal femur

3.4.1- General remarks

As indicated before, hip fracture is a health problem of enormous proportions. In addition the continuos growth in the elderly population can be expected to dramatically increase both the number and associated cost of hip fractures.

There is also considerable controversy as to whether a fracture of the hip should be considered a disease (related to the excessive loss of bone that is associated with osteoporosis), an accident (related to increased frequency or severity of trauma among the elderly) or both. Melton et al.(1988) concluded that the combination of reduced skeletal resistance to trauma and increased propensity for falling is an important determinant of risk. As a result, it appears that both loss of bone and trauma are necessary, but not independently sufficient, to cause these age-related fractures.

To date, hip fracture prevention efforts have been directed primarily toward the improvement of bone loss. However, since 90 percent of all hip fractures are caused by falls, an alternative and complementary approach to the prevention of hip fractures should focus on fall prevention or on reducing the injury potential of those falls that do occur.

Unfortunately, falls have proven remarkably resistant to prevention and the use of trochanteric padding to reduce the injury of a fall is still in the early phases of development. With respect to the mechanics of a fall, extensive research has been conducted on fall initiation. Besides the instability phase that results in loss of balance, a fall consist of three additional phases: 1) a descent phase; 2) an impact phase; 3) a post impact phase during which the subject comes to rest. However, little is known about the kinematics and dynamics of these three phases.

Since falling to the side and impacting on the hip raises the risk of hip fracture significantly, a fundamental variable which determines fracture risk is the force applied to the greater trochanter in a sideways fall. Many researchers have attempted to estimate the direction and the magnitude of this force and consequently use these data in the analysis of fracture.

3.4.2- Experimental results of a sideways fall

In the study by Backman (1957) many loading configurations were investigated experimentally to model a sideways fall. The picture shown in Fig.(3.5) has been chosen by many researchers because it produces fractures *in vitro* similar to those observed clinically. This configuration was meant to simulate the situation in which the patient falls to the side, with the soft tissue overlying the posterolateral aspect of the greater trochanter when coming in contact with the ground. The direction of the loads are such that the axes of the diaphysis and femoral neck formed an angle of 30 degrees, with the plane perpendicular to the applied loads.

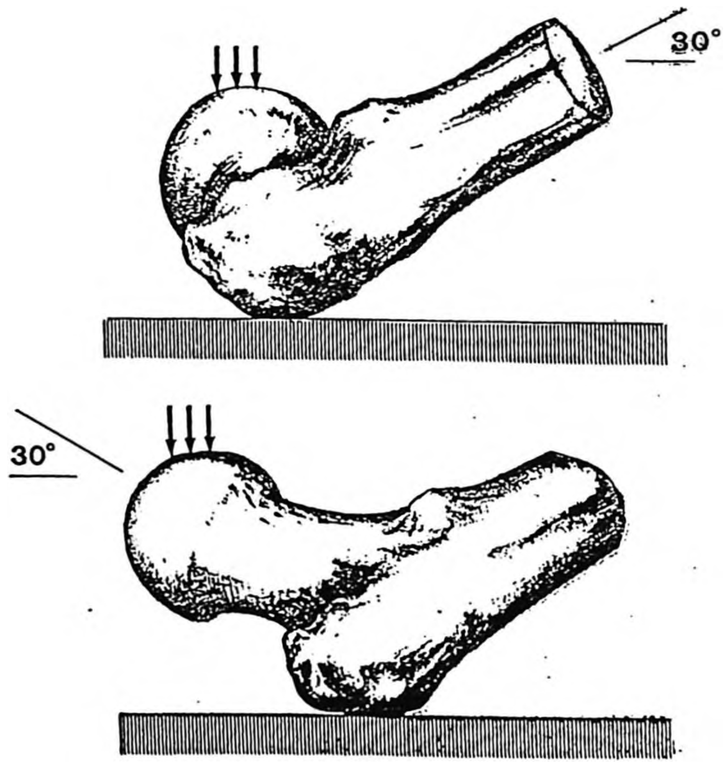

Fig.(3.5)
Loads applied to the femoral speciments
(from: Lotz et al., 1990)

Using above configuration, Lotz et al. (1991) performed an experiment to measure fracture load. In their tests, a vertical load was applied to the femoral head at a displacement of 0.7 mm/sec until failure occurred. The magnitude of applied load was measured by the calibrated load cell of the test system, while deformation of the specimen was measured with the calibrated linear variable-differential transformer of the hydraulic actuator. The resultant force-displacement diagram is shown in Fig.(3.6).

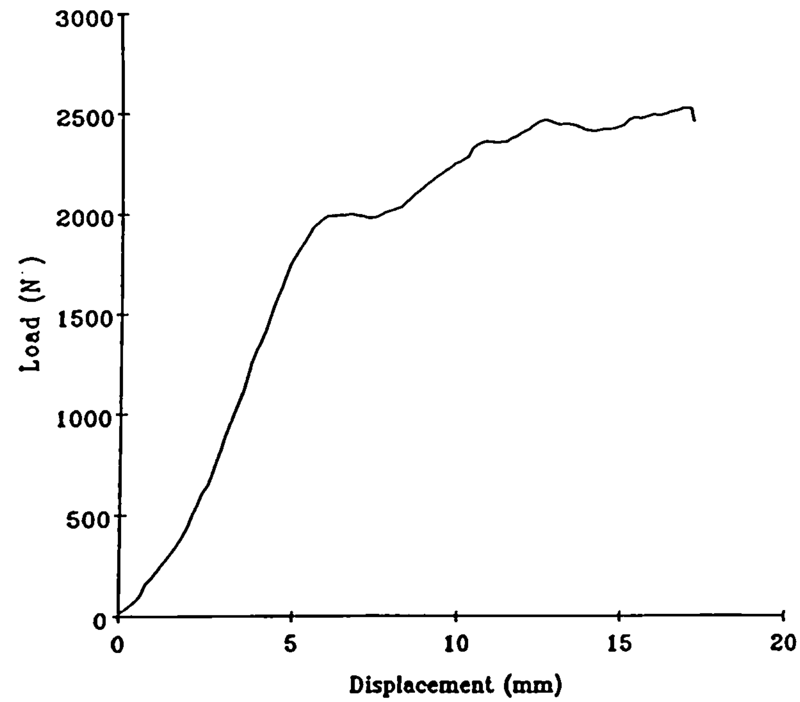

Fig.(3.6)

Load-deflection curve of a femur specimen

(From: Lotz et al., 1991)

In another experimental study, Keyak et al.(1997) investigated the magnitude of force in two different configurations for standing and falling. For standing load, force was applied to the femoral head and directed within the coronal plane at 20 degrees to the shaft axis. The contralateral femur was examined in a configuration simulating impact from a standing height similar to the loading investigated previously by Backman (1957).Fig.(3.7).The specimens were obtained from ten females and eight males between the ages of 52 and 92 . The results for fracture loads varied from 3 to 14 kN for standing configuration and 0.6- 4 kN for fall configuration.

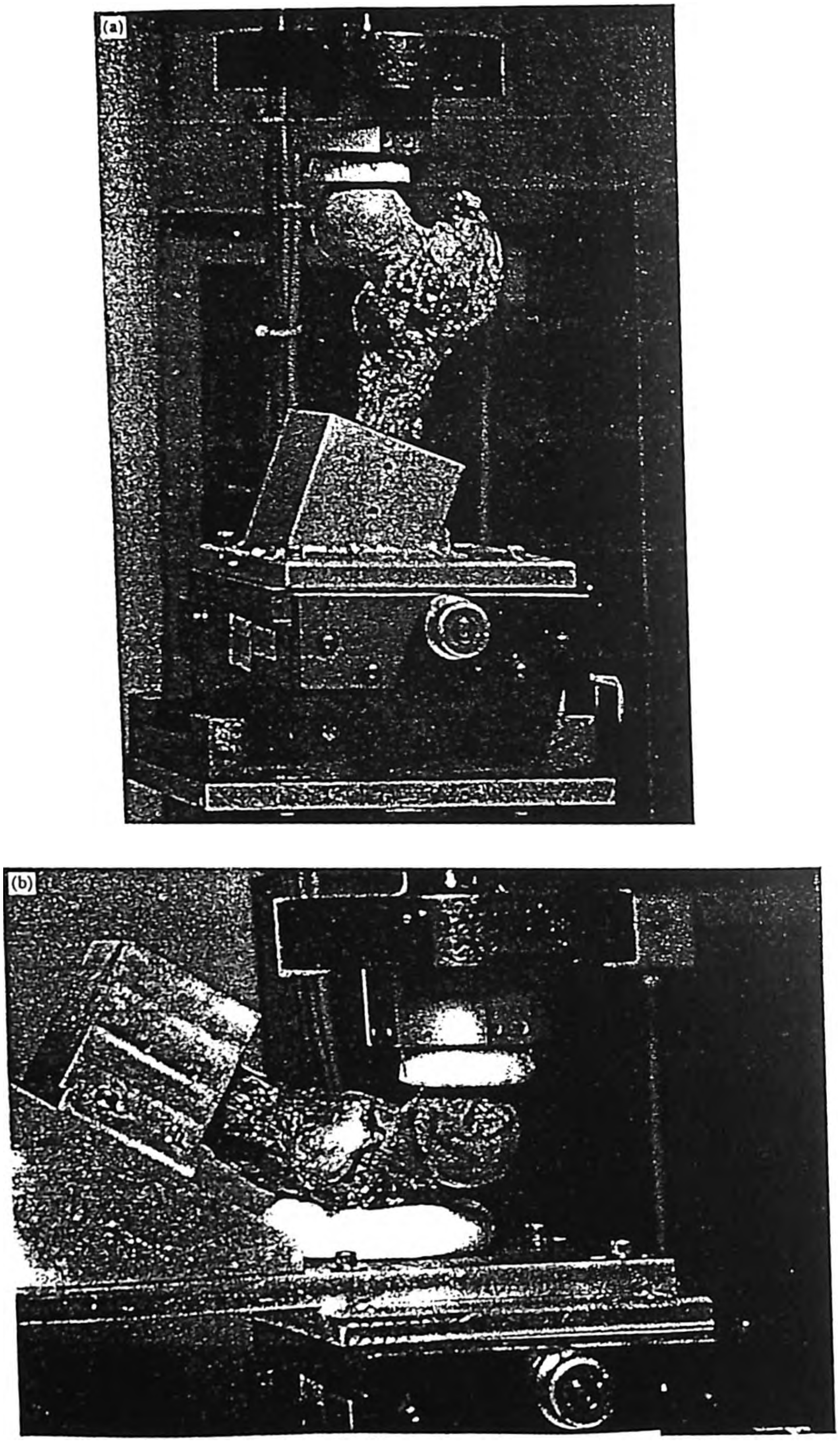

Fig.(3.7)

Experimental setups for testing the strength of the femur under different loading condition

(from: Keyak et. al, 1997)

Hayes et al.(1997) designed an experiment to calculate the highest force applied to the proximal femur during a fall. The physical system used in this study consisted of an impact pendulum and surrogate human pelvis, Fig.(3.8).

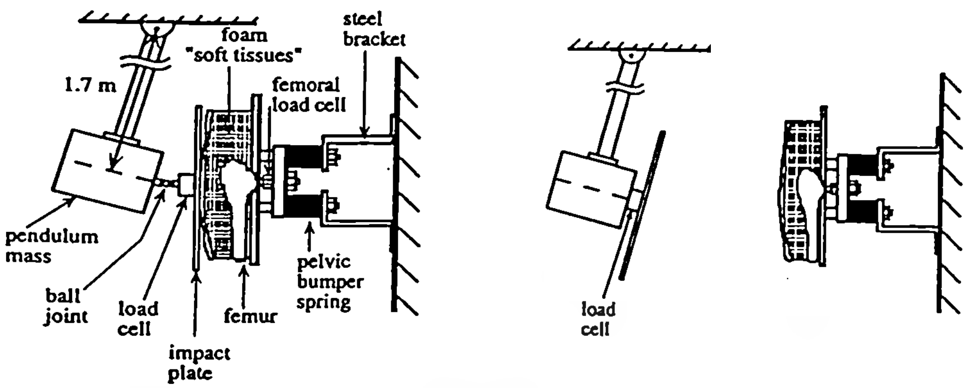

Fig.(3.8)

Physical system, consisting of a surrogate human pelvis and impact pendulum

(from: Hayes et al., 1997)

This system was used to simulate the dynamic response during impact to the lateral aspect of the hip resulting from a sideways fall. The compliance of the soft tissues (skin, fat, and muscle) overlying the femur and pelvis bone was simulated with polyethylene foam from rubber, while the stiffness and damping of pelvis was simulated using neoprene and bumper springs. The entire unit was rigidly mounted to a vertical wall. The pendulum was suspended from the ceiling by two low-friction ball bearings and consisted of an arm 1.74 m in length and ending on a rectangular weight cavity capable of holding up to 123 kg. A local cell mounted between the pendulum weight cavity and the impact plate provided a measure of the total force applied to the pendulum head, which consisted of two components: 1) the force delivered through the surrogate pelvis to the rear support wall; and 2) the inertial force associated with acceleration of the mass of the impact plate. The measured force-time record for the first contact period after the pendulum strikes the surrogate pelvis with a constant velocity of 2.22 m/s is shown in Fig.(3.9).

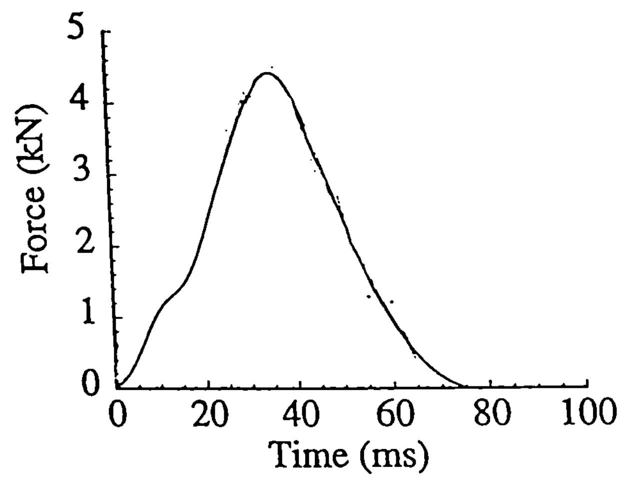

Fig.(3.9)
Experimental force-time record for a contact velocity u=2.22m/s
(from: Hayes et al., 1997)

3.4.3- Modeling of a fall

There is a number of studies which are focused on developing an equivalent dynamic model to predict the mechanical behavior of a femur. In a study by Van den Kroonenberg et al.(1995) a simple model is proposed to estimate the maximum force applied to the greater trochanter in the fall. The model is a single-degree-of-freedom system, which is shown in Fig.(3.10).

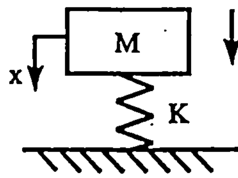

Fig.(3.10)
Single degree of freedom impact model
(from: Kroonenberg et al.,1995)

The mass M represents the mass of that part of the body that contributes to the impact force on the hip. According to this model, mass M is moving in the vertical direction with the velocity of V prior to impact. The spring, with the linear constant K, represents the soft tissue overlying the hip as well as the flexural stiffness of the body. Damping, however, is not considered in this model. To calculate M and V, three different schemes are proposed. See Fig.(3.11).

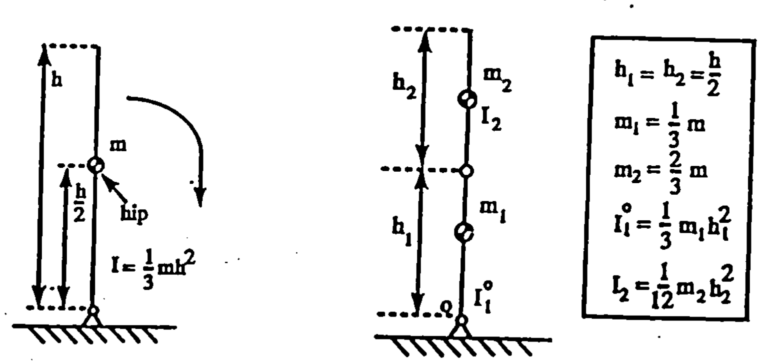

Fig.(3.11)
Rigid uniform slender bar and two link model
(from: Kroonenberg et al.,1995)

Different results based on the above mentioned model have been reported. Values for M ranged from 15.9 to 45.3 kg , while velocity (V) is estimated to have ranged from 2.47 to 4.00 m/s. Using these data and considering the stiffness (K) of 71 kN/m, the predicted values for peak impact force ranged from 2.90 to 7.5 kN.

In order to develop the previous method, a series of more complicated models have been proposed by Robinovitch et al.(1997). These models are shown in Fig.(3.12). The Voigt support model, (b), is used when damping is an important characteristic of the system. The Maxwell support model, (c), is not generally reliable, perhaps due to its prediction of a steady, non-zero rate of deformation under a steady load. In the standard linear solid support model, (d),techniques for quantifying the stiffness and damping constant are not as straightforward, and do not appear to have been documented previously. Consequently, a new formulation is proposed by authors. The predicted force-time records for these models are shown in Fig.(3.13) and are compared to the experimental results mentioned earlier.

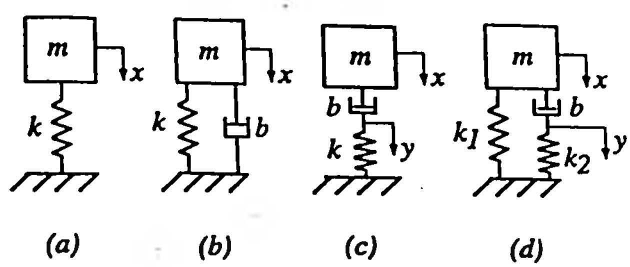

Fig.(3.12)
a) mass-spring model b) Voigt support model c) Maxwell support model and d) standard linear solid support model (From: Robinovitch et al.,1997)

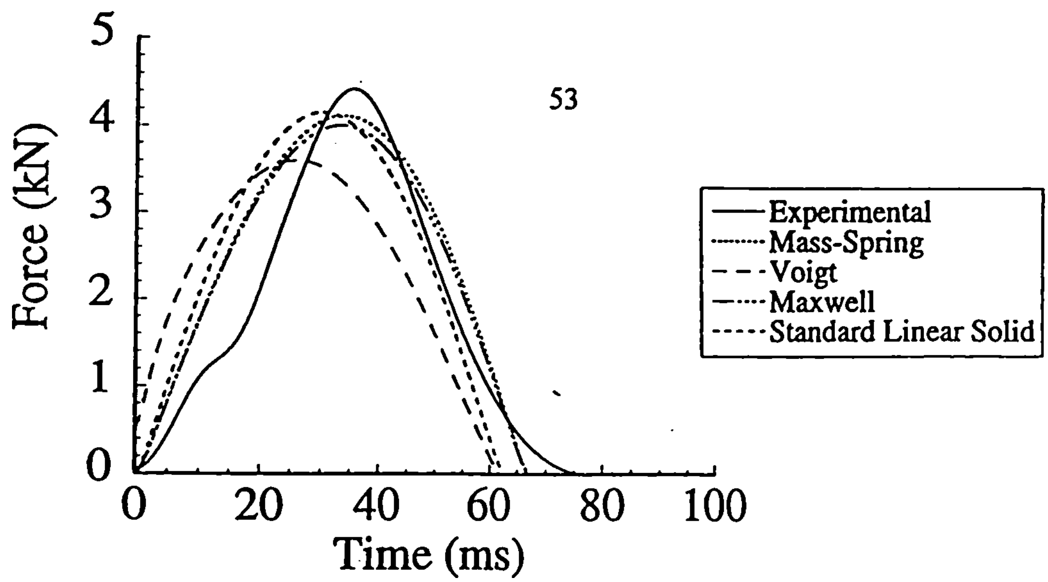

Fig.(3.13)
Measured and predicted force-time records for a contact velocity u=2.22 m/s
(From: Robinovitch et al.,1997)

3.4.4- Numerical approach

The application of the finite element method for both two and three dimensional analysis of the proximal femur is becoming a routine. Finite element method presents two main advantages over other techniques for the structural analysis of the proximal femur. The first advantage is that this method allows parametric representation of the complex geometric and material property distributions, which occur in vivo and which are normally difficult to represent with other analytical or experimental techniques. The second advantage, is that while an intact bone can be tested to failure once, a finite element model can be analyzed parametrically to investigate different loading conditions, geometries as well as material property distribution.

The studies by Elsasser et al. (1980), Revak (1998) and Genant et al. (1985) have demonstrated that quantitative computed tomography is an accurate technique for the assessment of intact bone status. Since then, much attention has been directed toward the development of various non-invasive screening procedures to measure bone geometry and the distribution of properties.

Lotz et al.(1991) used computed tomography to produce a finite element model to predict fracture of proximal femur. In their study, finite element models of intact proximal femurs were created using geometry and density data derived noninvasively from quantitative computed tomography images. Using this imaging modality, both the bone geometry and density were determined and finite element models were generated. These models were subsequently used to investigate the structural behavior of the proximal femur subject to loading conditions approximating a one-legged stance and sideway falling, Fig.(3.14).

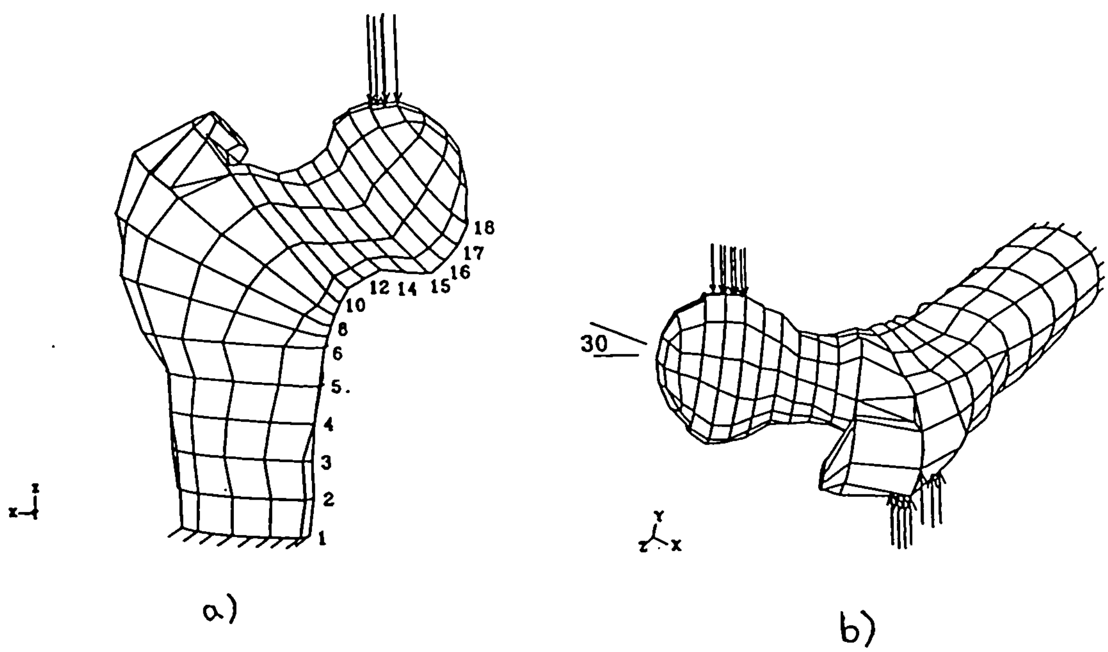

Fig.(3.14)
Loads applied to femur simulating a) one-legged stance and b)fall
(From: Lotz et al.,1991)

A distributed compressive load was applied to the superior aspect of the femoral head to approximate a one-legged stance. For the sideway falling configuration, a posterolaterally directed load was applied to the femoral head with an equal and opposite load applied to the lateral greater trochanter. To predict local bone failure, a von Mises yield criterion was used in the region representing cortical bone, and both von Mises and Hoffman yield criteria were applied for elements representing trabecular bone. The obtained load-displacement characteristics are shown in Fig.(3.15).

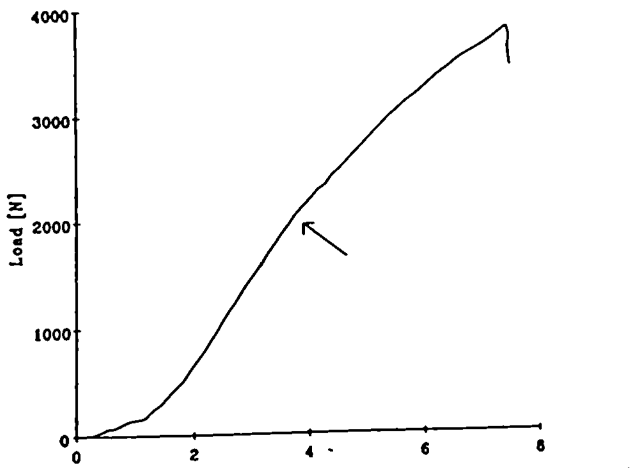

Fig.(3.15)
Load-displacement curve for a femur. The arrow indicates the approximate onset of yielding
(From: Lotz et al.,1991)

A similar approach was followed by Keyak et al. (1997). For finite element model generation, the CT scan data were transferred to a computer, and a 3-D finite element model, using heterogeneous linear isotropic mechanical properties, was automatically generated . Linear eight-nodded cube-shaped elements were used so that the elements matched the thickness of the CT scan images; See Fig.(3.16).The results of finite element analysis have been compared with the results of experiments; Fig.(3.17). It has been demonstrated that this technique can achieve precision comparable to that of densitometry and can predict femoral fracture load with very high accuracy.

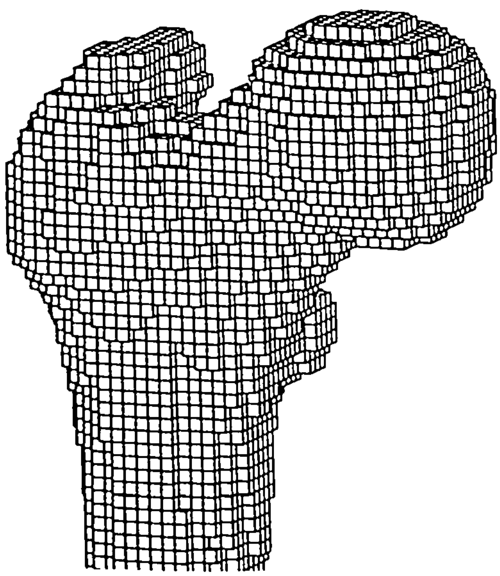

Fig.(3.16)
The finite element model of femur containing 14,534 nodes and 11,604 cube elements.
(from: Keyak et al.,1997)

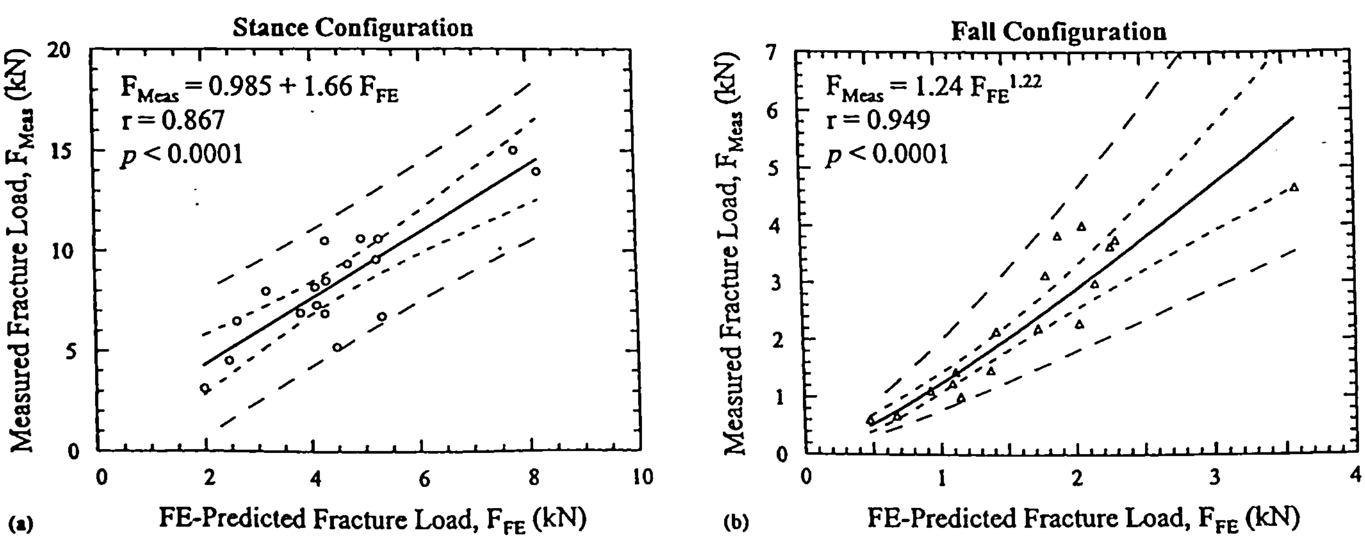

Fig.(3.17)
Measured fracture load versus FE-predicted fracture load for the stance configuration (a) and fall configuration(b).
(from: Keyak et al.,1997)

3.5- Present study

The analysis of bone fracture is quite complex. This arises from the fact that bone, both cortical and trabecular, is a heterogeneous and strongly anisotropic material. Previous studies (i.e Reilly and Burstien1975, Burstien et al 1976, Carter and Spengler ,1978, Torzilli et al.1981, Stone et al.,1983 and Keaveny et al.,1994) have clearly demonstrated that the mechanical behavior is, generally, inelastic and bimodular (i.e. the strength in tension is considerably lower than in compression).

In recent years, many three-dimensional finite element analyses have been performed to simulate fracture in the human proximal femur (Lotz et al.1991a, 1991b, McNamara et al. 1996, Mertz et al.,1996 and Taylor et al. 1996). Most of them have used simple fracture criteria which have been developed for a class of isotropic, porous cemented materials. In particular, some of these studies (Lotz et al.1991a,1991b and Mewtz et al. 1996) have used Von Mises failure criteria, which was primarily developed for metals. In more recent studies (i.e Pietruszczak et al.1999a), a new criterion for fracture of bone, both trabecular and cortical, has been proposed. This criterion was discussed in chapter 2 and will be employed later in this work to perform structural analysis of the proximal part of the femur.

The analysis performed in this study, incorporates a finite element model developed in the work of Pietruszczak et al.(1999a). The model has been created using COSMOS/M (1996) finite element software and several interface programs. The geometry of the femur was derived from external surface contours extracted from CT scans (512×512 pixels, pixel size: 0.219 mm, slice thickness: 1mm). The 204 consecutive images were scanned transversely to the long axis of the bone at 1mm intervals in the proximal femur and then at 7mm intervals along the diaphysis. The model consists of 9115 nodes and 40681 four-nodded tetrahedral elements.

The actual kinematics of a fall is very complex. Different researchers have reported quite diverse results regarding the estimation of maximum force due to the fall. A number of researchers (i.e. Lotz et al. 1991 , Keyak et al. 1997) did not consider the effect of tissues and used a simple static approach. However, the main source of inaccuracy comes from the fact that the force transferred during a fall is a dynamic force caused by impact. Thus, it will depend on many factors, such as, effective mass, velocity of impact, stiffness of the bone as well as the mechanical properties of tissue.

The work presented in this thesis is basically an extension of the work of Pietruszczak et al. 1999a.. The study has focused on two major areas. First, based on the formulation given in chapter 2 , a static analysis was performed for bone considered as a biphasic material. Second, the previous analysis was extended to the dynamic range, which describes more realistically, the conditions for a sideway fall.In next chapter, the details of static and dynamic analysis are explained and the results of numerical analyses are presented.

CHAPTER 4

Numerical simulation of fracture of proximal femur

4.1-Introduction

The numerical analysis presented in this chapter is basically a continuation of the previous study by Pietruszczak et al.(1999a). The analysis incorporates the finite element method and its objective is to model a fracture in proximal femur due to the sideways fall. The study presented in this thesis extends the previous analysis in two major areas. First, based on the formulation given in chapter 2, a static analysis was performed, taking into the account the biphasic nature of the material. The second contribution concerns the extension of the analysis to dynamic range, which simulates more closely the conditions of a sideways fall.

In this chapter, the method used for generating the finite element model, including geometry of femur and porosity distribution, is reviewed first. Subsequently, the details of the analyses and the results of both static and dynamic simulations are presented.

4.2- Geometry and physical properties of femur

In this section, the procedure used to generate the finite element model of the femur is outlined. The information is extracted from the work of Dean Inglis (Pietruszczak et. al,1999a).

The geometry of the femur has been obtained using CT scans and several processing techniques. The bone, that had been previously dried, was placed in a perspex cylinder filled with vegetable oil in order to simulate a soft tissue background during CT scanning. Images were scanned perpendicular to the long axis of the bone at 1 mm intervals. By using a boundary extraction program, external surface contours were obtained from each image. Contour pixels were mapped to the Cartesian reference frame and a subset of control points were chosen by visual inspection and connected to form a smooth contour. Consecutive contours were joined together to create three and four-sided surface patches. The final polyhedra were meshed into four noded tetrahedral elements using COSMOS/M (1996) finite element software. Fig.(4.1)shows the model of the femur which consists of 40681 tetrahedral elements and 9115 nodes.

The average density and porosity values were estimated from CT data by employing a simple algorithm which was used to calculate the values on an element by element basis. Fig.(4.2) shows the distribution of average porosity in the midcoronal plane.

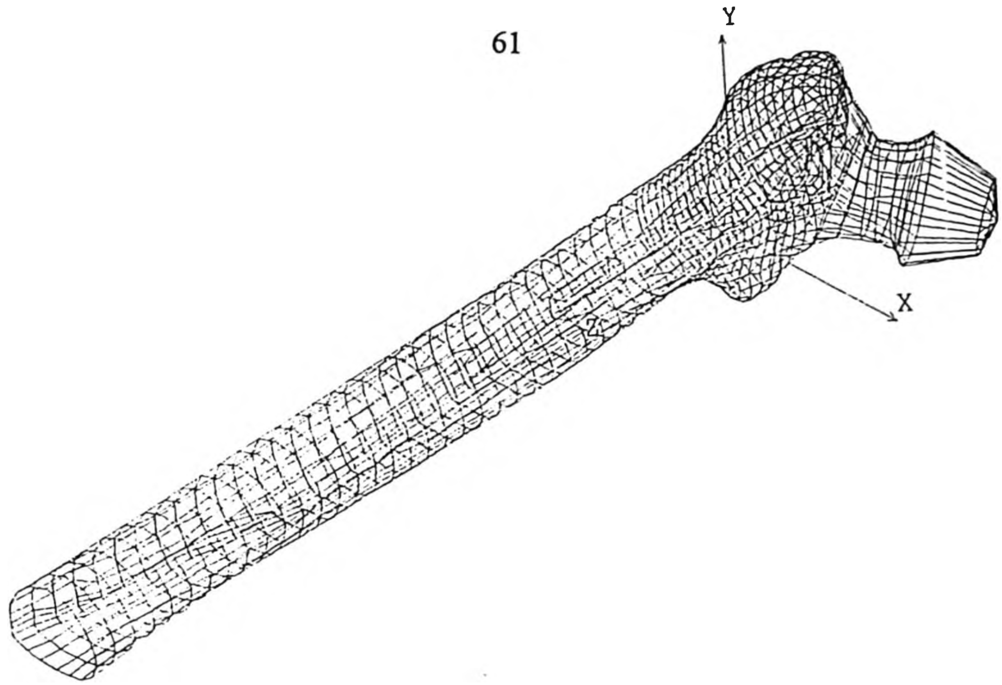

Fig.(4.1)
Finite element model of a femur
(From: Pietruszczak et. al,1999a)

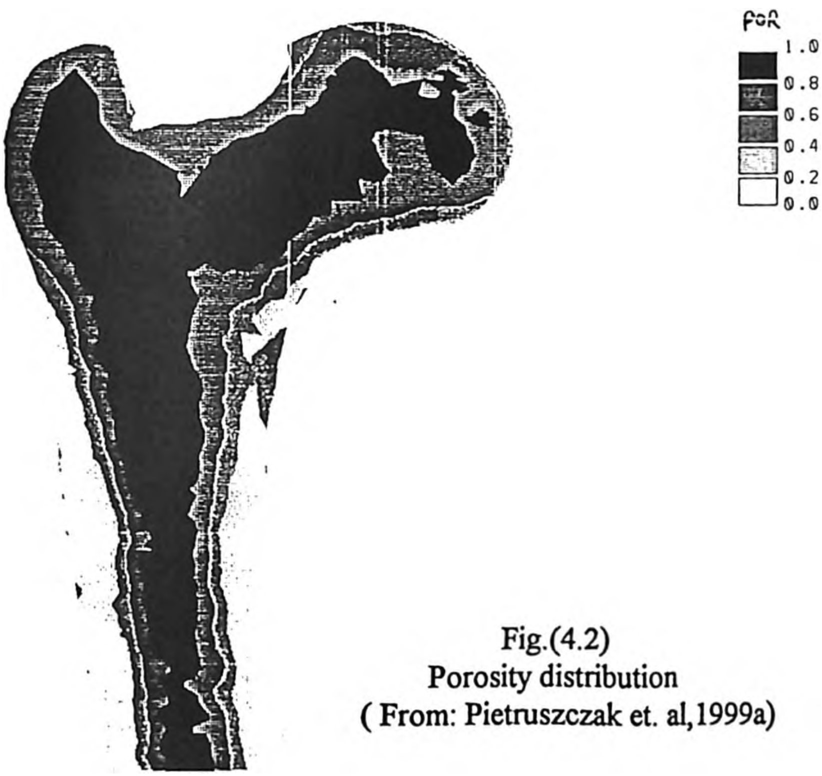

Fig.(4.2)
Porosity distribution
(From: Pietruszczak et. al,1999a)

To estimate the distribution of principal material directions, a preliminary finite element simulation was conducted . A linear analysis of femur subjected to loading conditions corresponding the one legged stance phase of gait was performed . The problem was solved under the constraint that the matrix multiplication of the stress and fabric tensors is commutative. The latter is consistent with Wolff's hypothesis, which states the principal stress axes coincide with the principal material directions at the remodeling equilibrium. The results for average porosity distribution and principal material directions were stored in input files which were subsequently used in the numerical analysis.

4.3- Static analysis of femur fracture

4.3.1- Material properties and loading

In order to maintain an orthotropic representation, a constant bias in the spatial distribution of voids was assumed by taking $\Omega_1 = -0.15$, $\Omega_2 = 0.04$, $\Omega_3 = 0.11$.

The elastic properties were estimated from eqs.(2.29) and (2.31) by taking

$\rho_b = 1.93\,\mathrm{g/cm^3}$, $E_o = 470\,\mathrm{MPa\,cm^6/g^2}$, $G_o = 180\,\mathrm{MPa\,cm^6/g^2}$,

so that for $n = 0.05$ there is: $E_1 = 19.76$ GPa, $E_2 = 13.15$ GPa, $E_3 = 11.15$ GPa,

, E_3 = 11.15 GPa , G_{12} = 6.6 GPA, G_{13} = 5.72 GPA , G_{23} = 4.71 GPA,

μ_{12} = 0.25, μ_{12} = 0.25, μ_{12} = 0.25 The above estimates are quite consistent with the data for human femoral cortical bone, as reported by Turner and Cowin (1998).

The loading configuration for static analysis was the same as that employed by Pietruszczak et al.(1999a). A load of magnitude 750 N was distributed among surface nodes of the lateral aspect of the grater trochanter. An equal and opposite load was applied to the femoral head in a similar manner.

For static analysis nodes at the distal end of femur were rigidly fixed. Such constraint was considered reasonable since the focus of loading activity was is in the proximal end of the femur. Previous studies (e.g. Vichnin et al. 1986) have shown this to be of little influence on the stress field in the proximal region. The loading configuration and kinematic constraints are shown in Fig.(4.3).

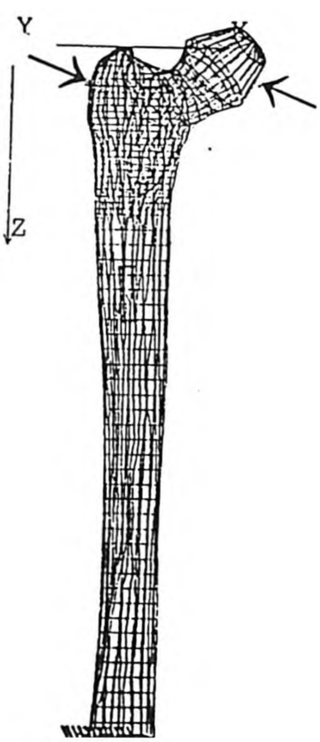

Fig.(4.3)
Loading configuration and kinematic constraints

The stress analysis was performed for different conditions including dry and wet bone, isotropic and orthotropic characteristics as well as two different porosity distributions corresponding to normal and osteoporosis bone.To assess the risk of fracture, the concept of *damage factor*, suggested by Pietruszczak et al.(1999a), was used. The damage factor is defined as:

$$\beta = \frac{\bar{\sigma}}{g(\theta)\bar{\sigma}_c} \tag{4.1}$$

where $\bar{\sigma}$, $g(\theta)$ and $\bar{\sigma}_C$ are all defined in equation (2.17) in chapter2. It should be noted that, according to equation 2.17, $F \leq 0$ requires $0 \leq \beta \leq 1$. The case of $\beta \to 1$ results in $F \to 0$ which signifies the local failure of the bone material. Generally, the distribution of β shows the extent of structural damage and identifies the regions where the irreversible deformation are likely to occur.

4.3.2- Results of static analysis

In this section the results of static analysis, based on the formulation given in chapter 2, are presented. The analysis was performed for different cases, including isotropic/orthotropic material and dry/wet bone. In what follows the results of simulations are discussed in details.

Fig(4.4) shows the finite element mesh for the femur and the location of anterior cross section. Based on experimental evidence, the femur fracture usually initiates along this section.

In Fig(4.5) the damage factor distribution in a dry healthy bone is shown for two different cases a) orthotropic and b) isotropic material. The results for both cases indicate that the high stress concentrations occur in femoral neck which is in tension. The magnitude of damage factor is less than one, implying that no fracture is expected. The comparison of orthotropic and isotropic case shows that the extent of damage is slightly higher in orthotropic material. Overall, however, the distribution is very similar. This is true, provided the isotropic properties are taken as the orientation average corresponding to orthtropic case(i.e $\Omega_{ij} = 0$).

Fig(4.6) shows the damage factor distribution in dry osteoporotic bone for a)orthotropic and b)isotropic case. The higher values of damage factor for orthotropic material are consistent with the results shown in Fig(4.5). It can be seen that in the area of femoral neck there is $\beta \geq 1$, which indicates the onset of fracture. Thus the values of the damage factor for osteoporotic bone are significantly higher than those corresponding to a healthy bone. Note that in the analysis the bone material is considered to be linearly elastic, which is not a valid assumption for region experiencing $\beta \geq 1$. However, the elastic solution can be a useful factor to assess the plastic admissibility of the stress state, and thus, the risk of fracture.

The higher risk of fracture in osteoporotic bone is clearly evident in Fig(4.7). The figure shows the damage factor distribution corresponding to orthotropic biphasic (wet) material in a) healthy and b) osteoporotic bone. The damaged regions in both cases are located in femoral neck. The results are consistent with clinical data indicating higher rate of femur fracture in elderly and the onset of fracture in femoral neck.

Fig.(4.8) shows the distribution of damage in midcoronal section for a)healthy and b)osteoporosis orthotropic bone. The figure shows that in a healthy bone the extend of damage is limited so that no fracture is expected. Fig. (4.8 b) shows a significant increase in damaged area in osteoporotic bone. In this case, the damage extends to the trabecular bone in interior part. This is mainly due to the fact that porosity in trabecular region is very high, so that even a small increase in external load can cause a rapid propagation of fracture.The latter is further confirmed in Fig.(4.9) which shows the anterior section of a) normal and b) osteoporotic orthotropic wet bone. In Fig.(4.9 b) the extent of damage in both tension and compression regime is much more severe and is due to the increase in porosity of aged bone. As indicated before, increase in porosity leads to a significant decrease in the stiffness and the strength of the material.

Fig.(4.10) shows the damage factor distribution in a) dry and b) wet isotropic healthy bone. The results indicate that, the damaged area in femoral neck is almost identical for both these cases. The similarity of results in dry and wet conditions can be explained by reviewing the formulation for biphasic material, as discussed in chapter 2. The fluid affects the behavior when the material is under compression as it cannot, in general, sustain the tension beyond the atmospheric level. Thus, in problems involving femur fracture, where damage occurs in tension, the significant changes in damage factor distribution are not expected. This is further confirmed in Fig.(4.11), which shows anterior view of the bones. The damage factor distribution is different in compression area (right side of picture), but almost identical in tension region.

Fig.(4.12) shows the damage factor distribution in a)dry and b) biphasic osteoporotic bone. Comparing this figure with Fig.(4.10), it is evident that under osteoporotic conditions, the damage factor is significantly higher than that corresponding to a healthy bone. However, the changes in damage factor between dry and biphasic materials are small and the difference, again, appeares in compression regime.

The anterior views of a)dry and b)biphasic osteoporotic bone are shown in Fig.(4.13). There again, the damaged area is almost the same for dry and biphasic conditions, and the difference occurs only in compression regime(right side of cross section). The results are consistent with those for a healthy bone, Fig.(4.10) and (4.11).

Fig.(4.14) presents the excess pore pressure and mean stress distribution in a wet healthy bone considered as orthotropic material. The units are MPa and the negative values indicate compression. In general, the distribution of excess pore pressure, Fig.(4.14 a), is consistent with the mean stress distribution, Fig.(4.14 b). Since the excess pore pressure is generated only in compression area, the zero pore pressure line indicates the border between tension and compression regime. The location of this line is consistent with the contour zero mean stress, in Fig.(4.14 b).

Finally, Fig.(4.15) shows the distribution of a) excess pore pressure and b) mean stress for osteoporosis bone(isotropic case). Comparison of this figure with Fig.(4.14), indicates that mean stress distribution and pore pressures are almost the same for both normal and osteoporotic bone. The primary reason that osteoporosis case shows more damage is due to higher porosity of the material.

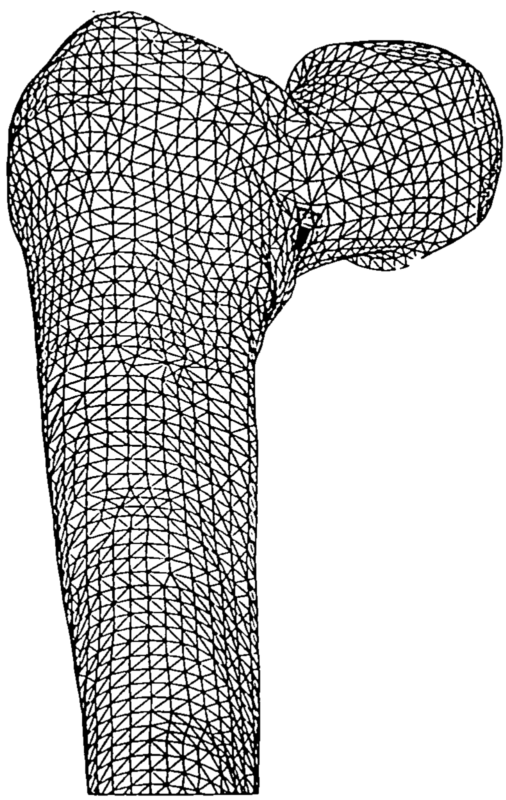

Fig.(4.4)

A general view of finite element mesh and anterior cross section(a-a)

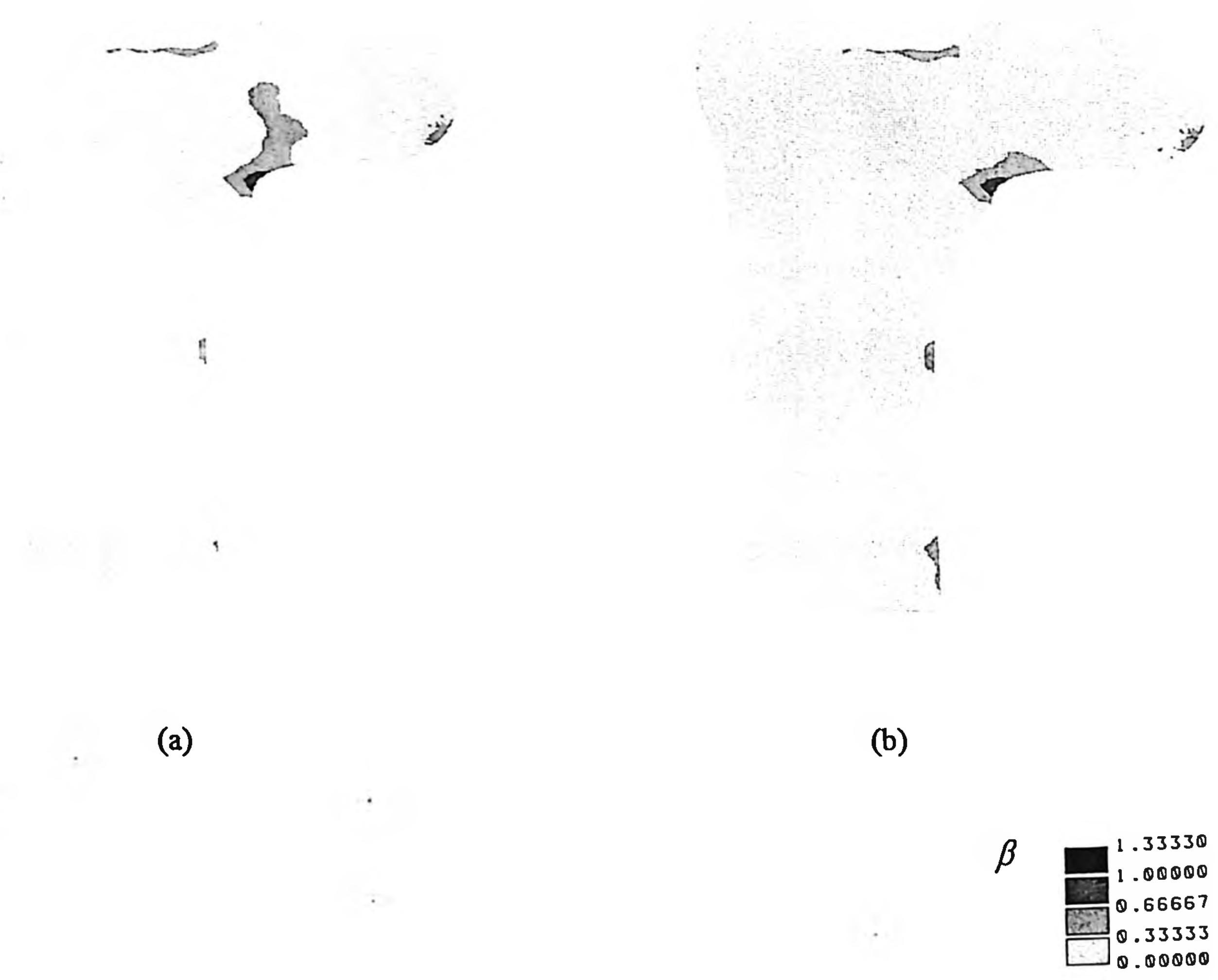

Fig.(4.5)

Damage factor (β) distribution in a) orthotropic and b)isotropic dry normal bone (static analysis: midcoronal plane)

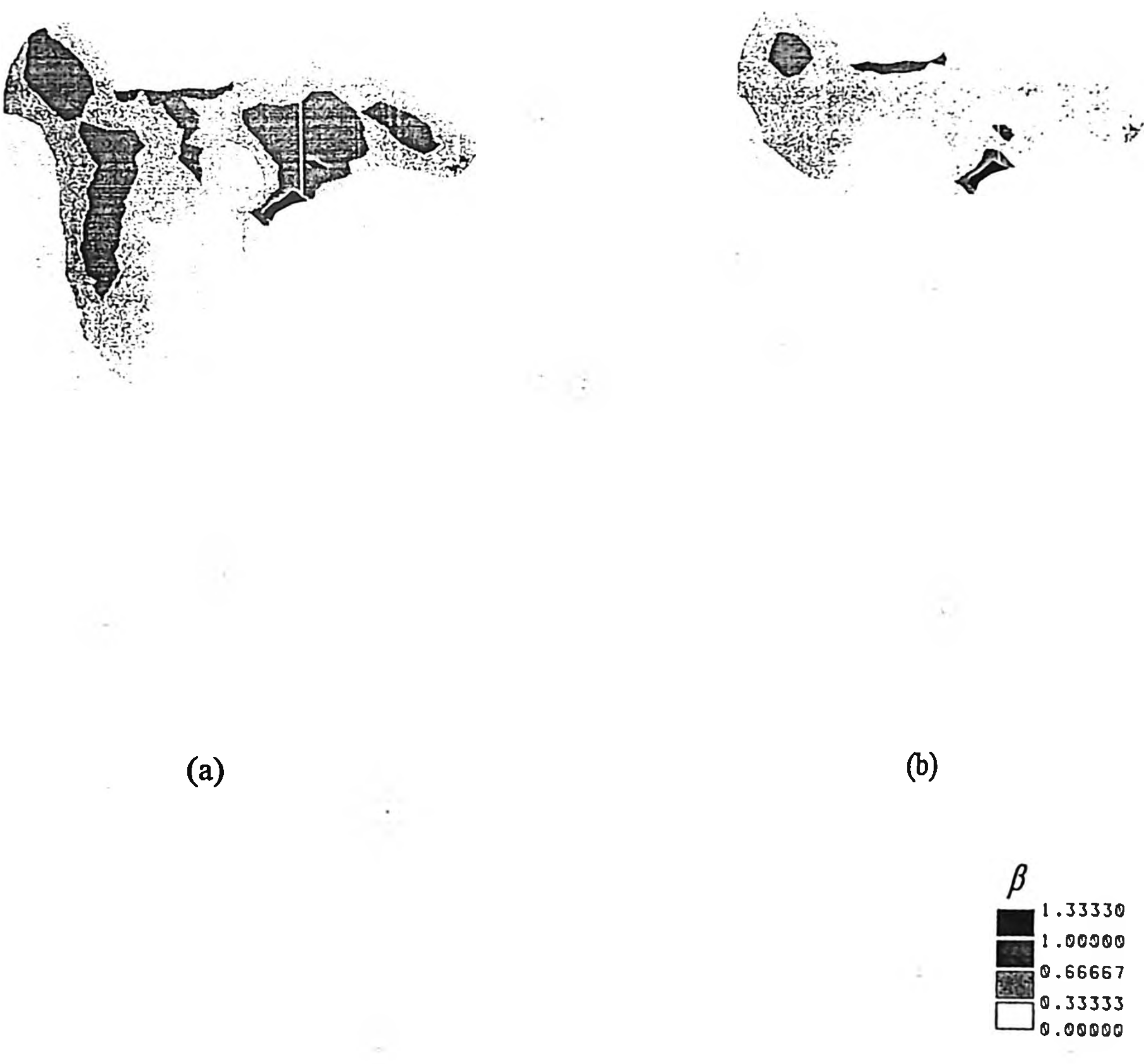

Fig.(4.6)

Damage factor (β) distribution in a) orthotropic and b)isotropic dry osteoporosis bone (static analysis: midcoronal plane)

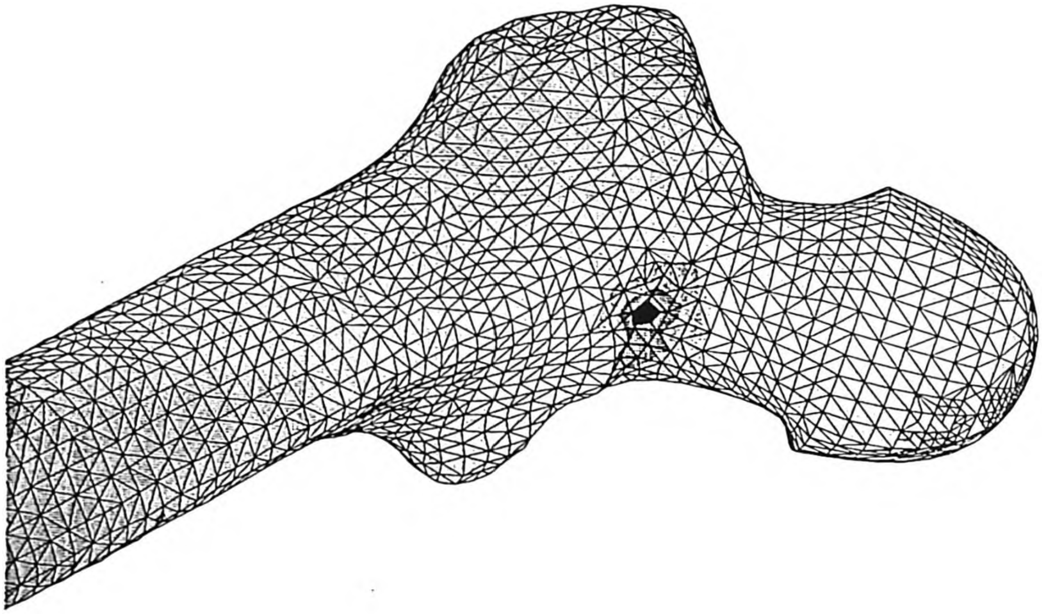

a)

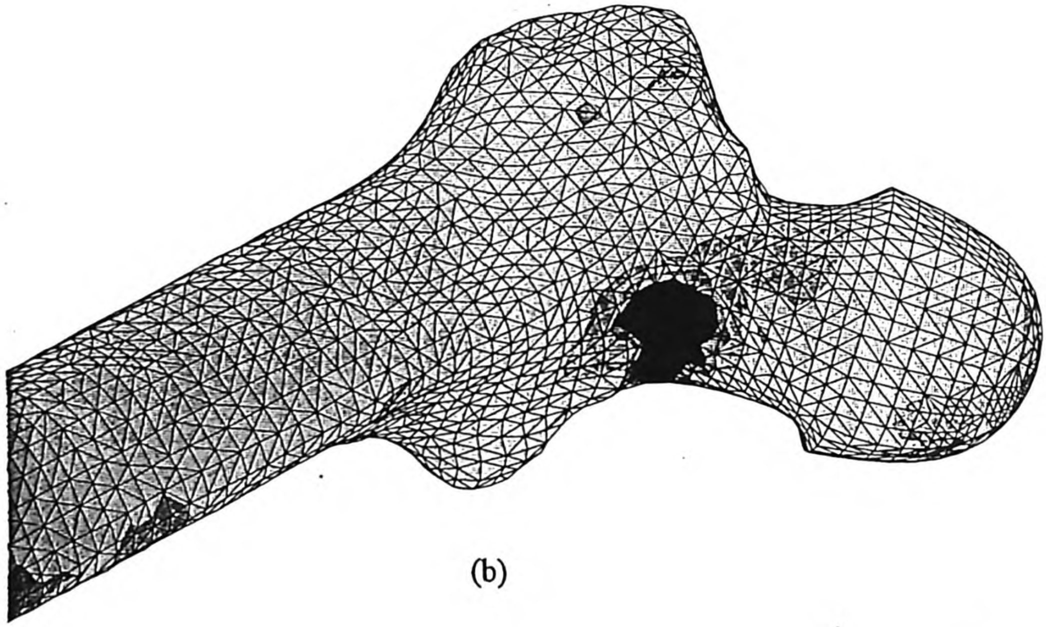

(b)

Fig.(4.7)

Damage factor (β) distribution in a) normal and b)osteoporosis orthotropic wet bone (static analysis)

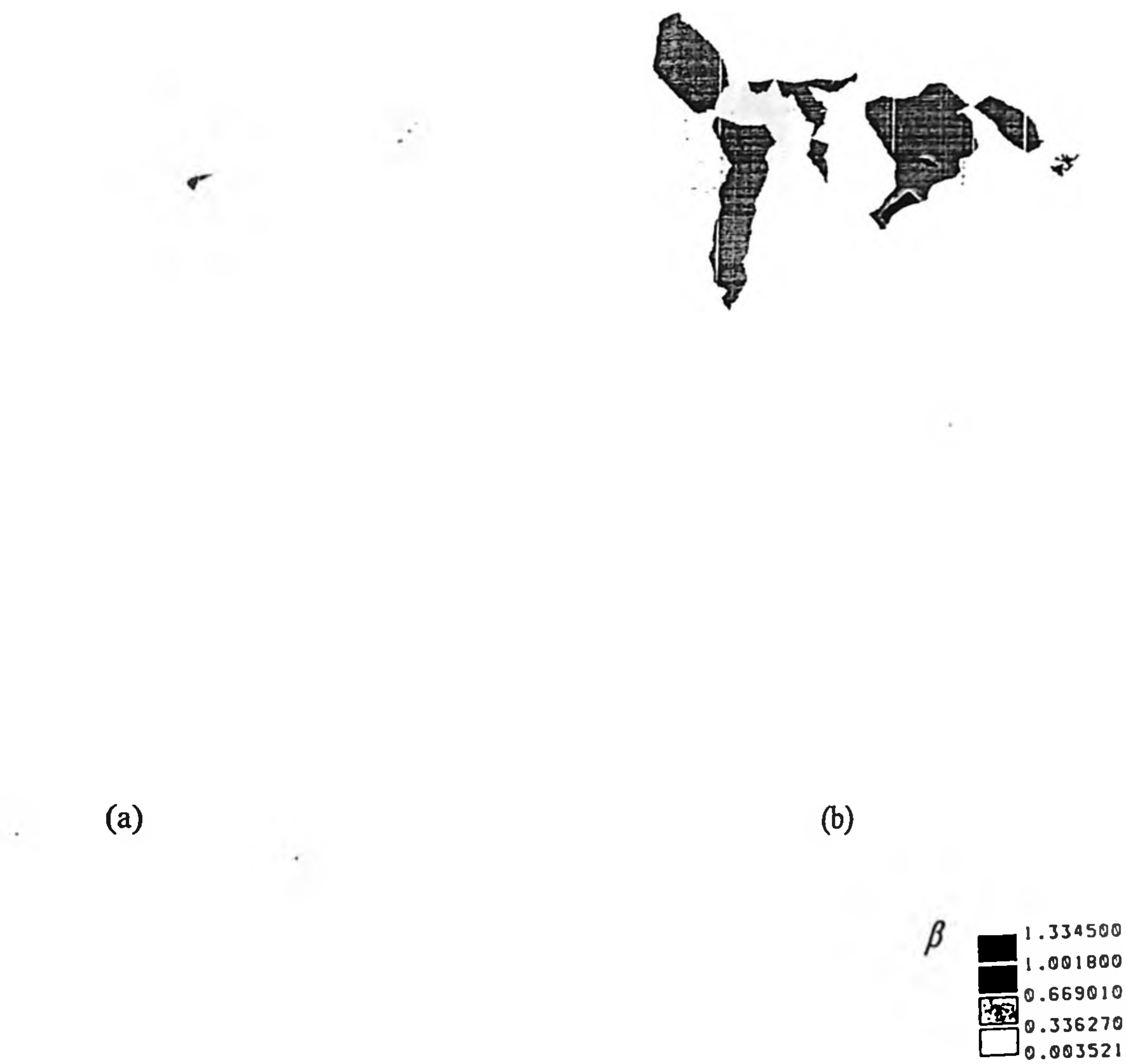

Fig.(4.8)

Damage factor (β) distribution in a) normal and b)osteoporosis orthotropic wet bone (static analysis: midcoronal plane)

(a)

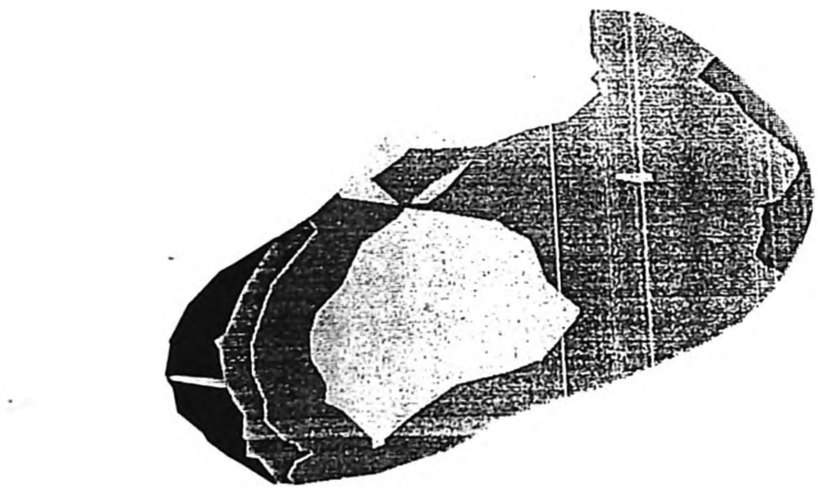

(b)

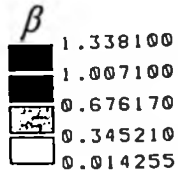

Fig.(4.9)

Damage factor (β) distribution in a) normal and b)osteoporosis orthotropic wet bone (static analysis: anterior view)

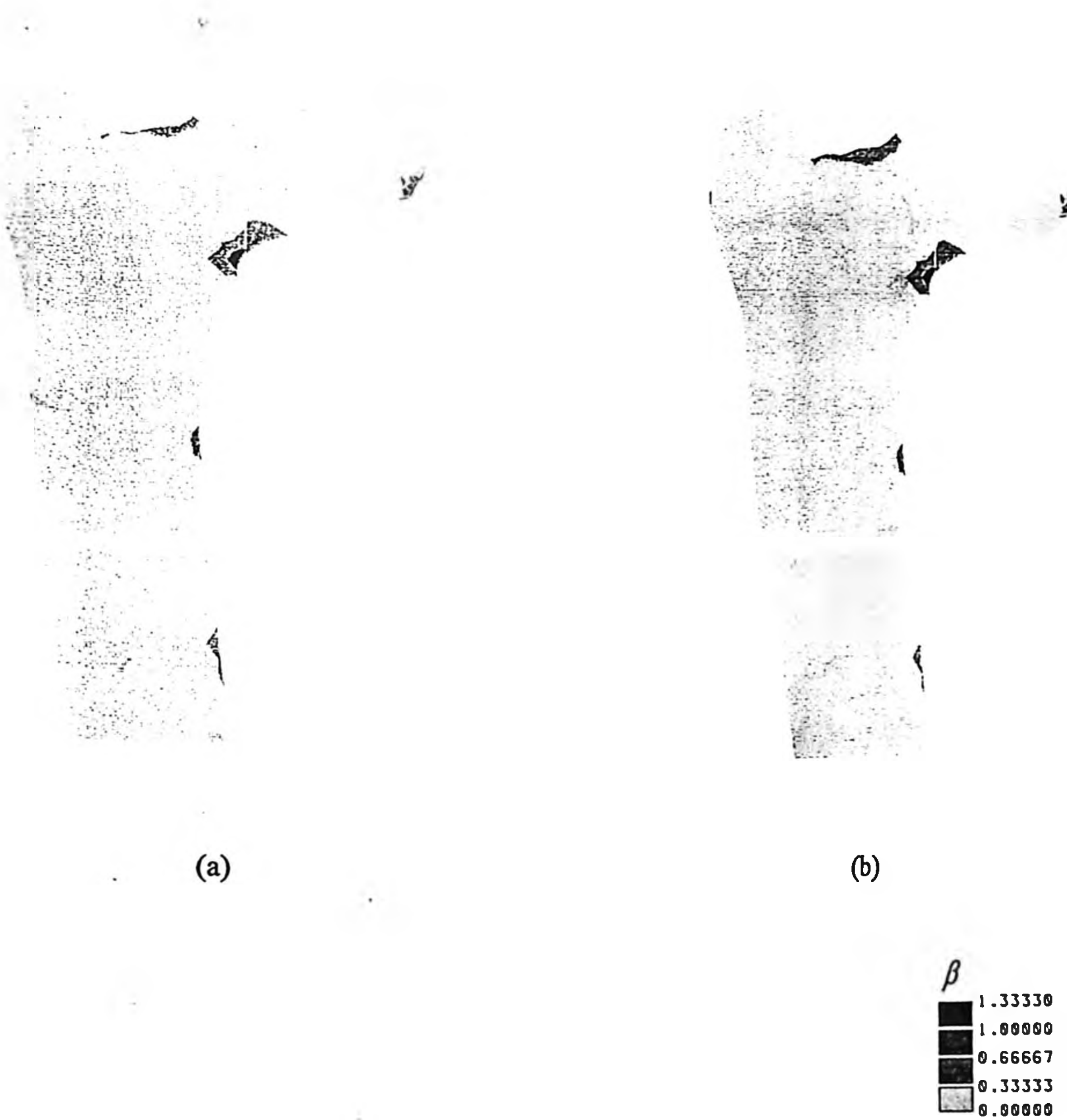

Fig.(4.10)

Damage factor (β) distribution in a) dry and b)wet isotropic normal bone
(static analysis: midcoronal plane)

(a)

(b)

Fig.(4.11)

Damage factor (β) distribution in a) dry and b)wet isotropic normal bone (static analysis: anterior view)

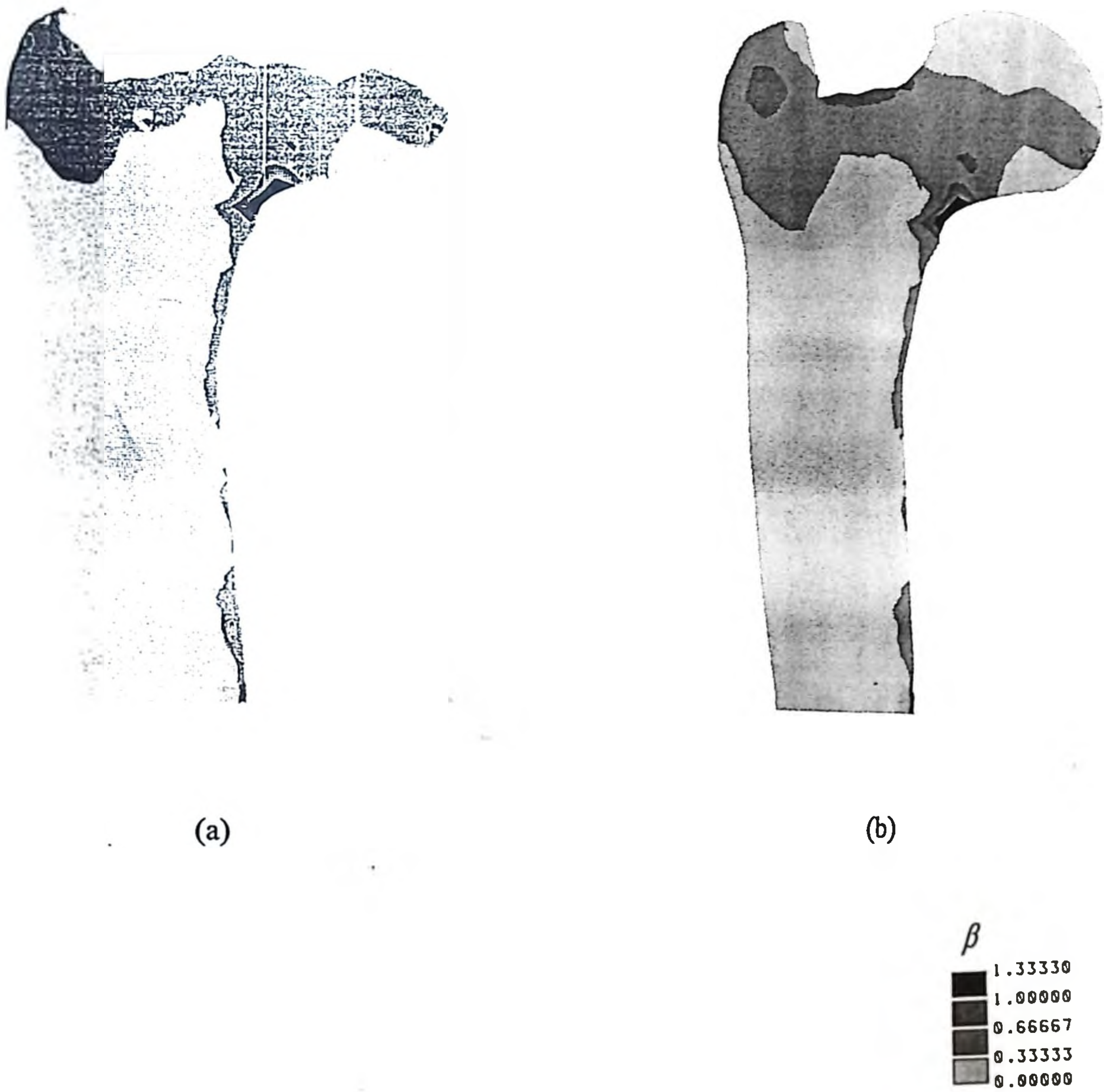

(a) (b)

Fig.(4.12)

Damage factor (β) distribution in a) dry and b)wet isotropic osteoporosis bone
(static analysis: midcoronal plane)

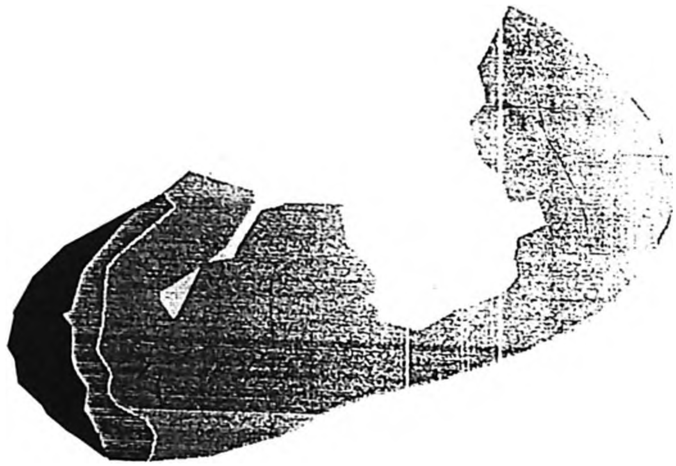

(a)

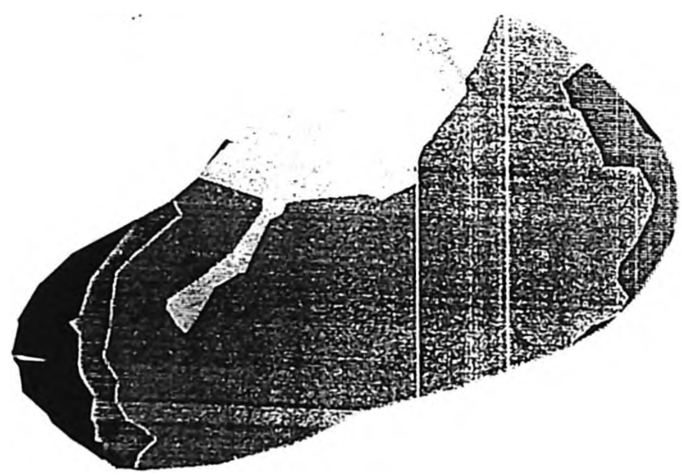

(b)

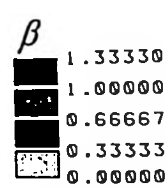

Fig.(4.13)

Damage factor (β) distribution in a) dry and b)wet isotropic osteoporosis bone
(static analysis: anterior plane)

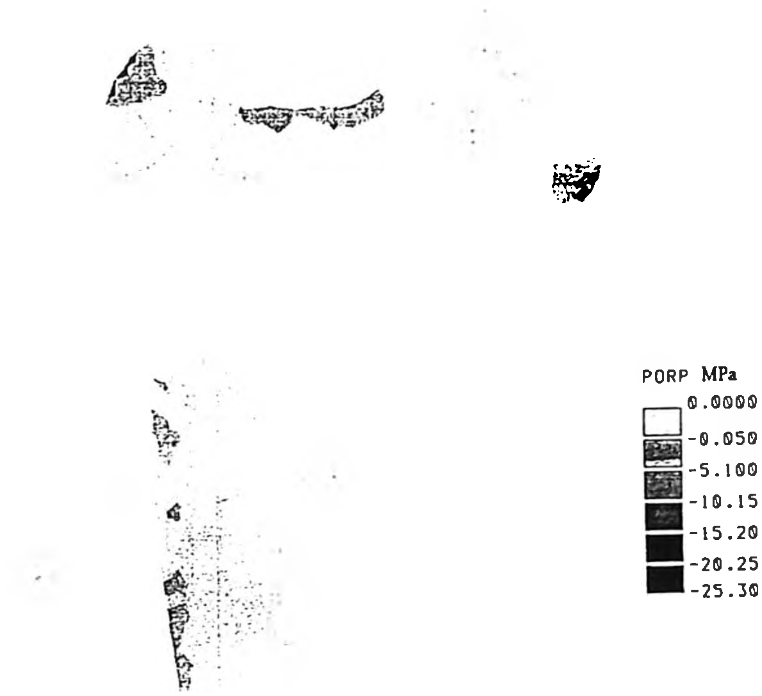

(a)

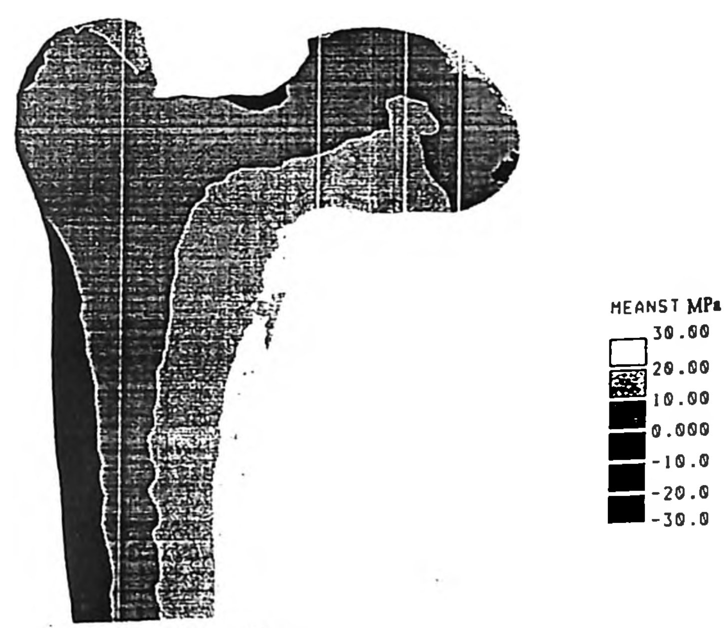

(b)

Fig.(4.14)

a) excess pore pressure and b)mean stress of orthtropic wet normal bone
(static analysis: midcoronal plane)

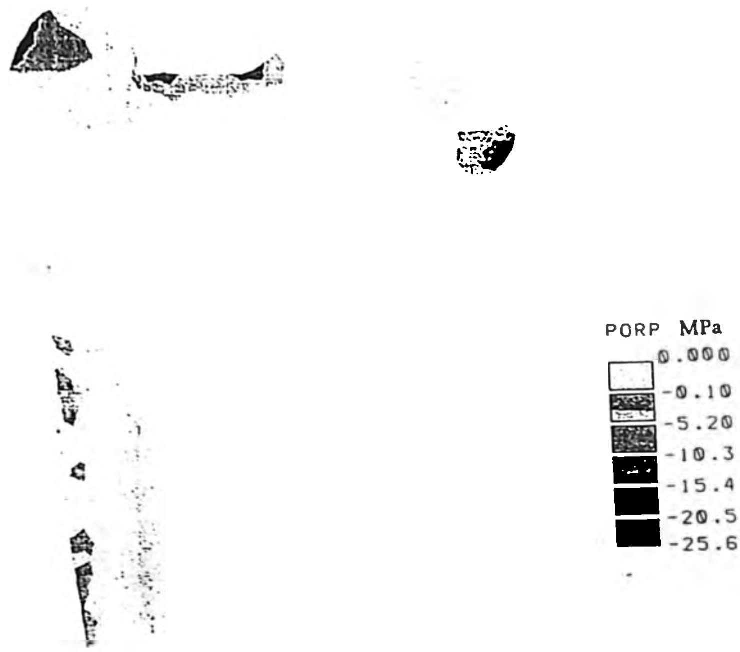

(a)

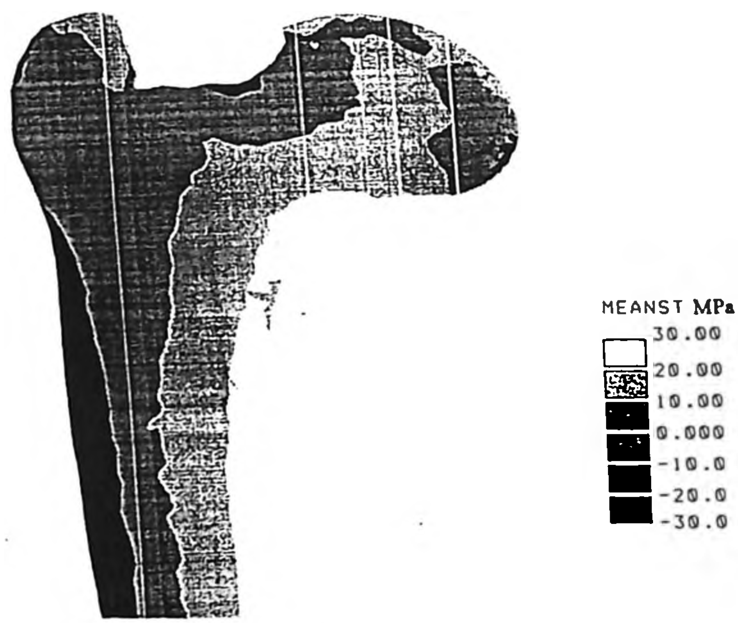

(b)

Fig.(4.15)

a) excess pore pressure and b)mean stress of isotropic wet osteoporosis bone (static analysis: midcoronal plane)

4.4-Dynamic analysis of fracture

4.4.1-Finite element methods in dynamic analysis

The equations of motion for a linear dynamic system are:

$$[M]\,\{U\}+[C]\,\{\dot{U}\}+[M]\,\{\ddot{U}\}=\{f(t)\} \qquad (4.2)$$

where;

$[M]$ - mass matrix
$[C]$ - damping matrix
$[K]$ - stiffness matrix
$\{f(t)\}$ - time varying load vector

and $\{U\}$, $\{\dot{U}\}$, $\{\ddot{U}\}$ are the nodal displacements, velocities and accelerations, respectively. Many different methods have been proposed to solve the set of above equations, among them *modal analysis* is more commonly used. In this approach, the system of equations of motion is decoupled into n single degree of freedom equations in terms of the modal displacement vector $\{x\}$, such that

$$\{U\} = [\Phi]\{x\} \qquad (4.3)$$

where $[\Phi]$ is the matrix of the lowest n eigenvectors obtained from the solution of:

$$[K]\{U\} = \omega^2[M]\{U\} \qquad (4.4)$$

Substituting equation (4.3) into equation (4.2) and multiplying it by $[\Phi]^T$ results in

$$[\Phi]^T[M][\Phi]\{\ddot{x}\}+[\Phi]^T[C][\Phi]\{\dot{x}\}+[\Phi]^T[K][\Phi]\{x\}=[\Phi]^T\{f(t)\} \qquad (4.5)$$

The eigenvectors are M-orthonormal, i.e. they satisfy

$$\Phi^T M\Phi = I \quad , \quad \Phi^T K\Phi = \omega_i^2 \quad \text{and} \quad \Phi^T C\Phi = 2\omega_i\xi_i\delta_{ij} \qquad (4.6)$$

where I is the unit matrix, ξ_i is a modal damping parameter and δ_{ij} is the Kronecker delta. With the mode shapes satisfying the orthogonality conditions, eq.(4.5) becomes:

$$\{\ddot{x}_i\}+2\xi_i\omega_i\{\dot{x}_i\}+\omega_i^2\{x_i\}=\{\Phi\}_i^T\{f(t)\} \qquad (4.7)$$

The solution to the equation (4.7) can be obtained by employing standard procedures for the solution of differential equations with constant coefficients. In finite element analysis, there are several numerical techniques available. These techniques are developed based on two approximation. First, instead of satisfying time dependent equation(4.2) at any time t, it is satisfied only at discrete time intervals Δt. The second approximation is that a variation of displacements, velocities and accelerations within each time interval Δt is assumed.

There are several different integration algorithms, among which *Houbolt method*, *Wilson θ method* and *Newmark method* are most commonly used. In what follows the *Newmark method*, which is employed in this study, is briefly reviewed.

The Newmark method- In this method, the following assumptions are used: (Bathe, 1982)

$$\left\{\dot{U}_{t+\Delta t}\right\} = \left\{\dot{U}_t\right\} + \left[(1-\delta)\left\{\ddot{U}_t\right\} + \delta\left\{\ddot{U}_{t+\Delta t}\right\}\right]\Delta t \tag{4.8}$$

$$\left\{U_{t+\Delta t}\right\} = \left\{U_t\right\} + \left\{\dot{U}_t\right\}\Delta t + [(\frac{1}{2} - \alpha)\left\{\ddot{U}_t\right\} + \alpha\left\{\ddot{U}_{t+\Delta t}\right\}]\Delta t^2 \tag{4.9}$$

In above equations α and δ are the parameters that can be determined to obtain the desired integration accuracy and stability. For an unconditionally stable scheme , Newmark originally proposed $\delta = \dfrac{1}{2}$ and $\alpha = \dfrac{1}{4}$.

The equilibrium equation (4.2) at time $t + \Delta t$ can be written as

$$[M]\left\{\ddot{U}_{t+\Delta t}\right\} + [C]\left\{\dot{U}_{t+\Delta t}\right\} + [K]\left\{U_{t+\Delta t}\right\} = \left\{R_{t+\Delta t}\right\} \tag{4.10}$$

Solving from equation (4.9) for $\left\{\ddot{U}_{t+\Delta t}\right\}$ in terms of $\left\{U_{t+\Delta t}\right\}$, and then substituting $\left\{\ddot{U}_{t+\Delta t}\right\}$ into equation (4.8), we obtain the expressions for $\left\{\ddot{U}_{t+\Delta t}\right\}$ and $\left\{\dot{U}_{t+\Delta t}\right\}$ in terms of unknown displacements $\left\{U_{t+\Delta t}\right\}$ only. These two relations for $\left\{\ddot{U}_{t+\Delta t}\right\}$ and $\left\{\dot{U}_{t+\Delta t}\right\}$ are then substituted in equation (4.10) to solve for $\left\{U_{t+\Delta t}\right\}$, after which $\left\{\ddot{U}_{t+\Delta t}\right\}$ and $\left\{\dot{U}_{t+\Delta t}\right\}$ can be calculated from equations(4.8) and (4.9).

4.4.2- Finite element model

The dynamic finite element model which has been used for numerical analysis of fracture of proximal femur, is shown in the Fig.(4.16).The model employs a set of simplifying assumptions. In what follows, theses assumptions are discussed in the context of previous studies.

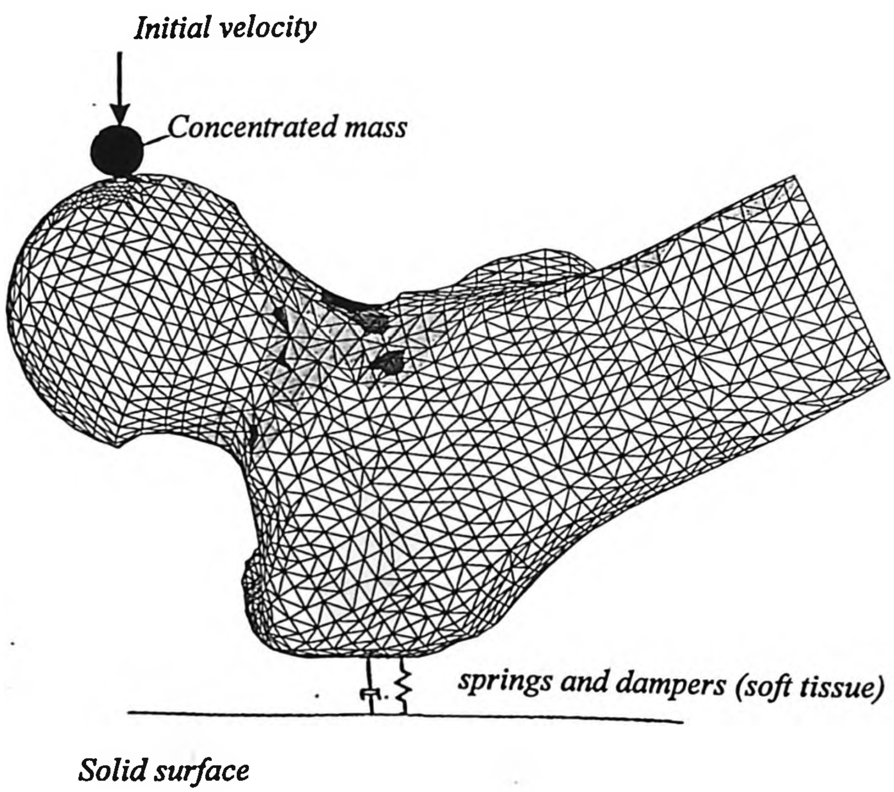

Fig.(4.16)
Dynamic finite element model

Body configuration in falling

As mentioned in chapter 3,many different loading configurations corresponding to a fall, have been investigated experimentally. Among those, the configuration suggested by Backman (1957), Fig (3.5), has been used by many researchers, since it produces fractures similar to those observed clinically. This configuration was employed in the present study in terms of specifying the direction of the initial velocity as well as the kinematic constraints in contact area.

Effective mass

The effective mass is the mass of that part of the body that is moving prior to impact. Much of research effort has been devoted to estimate the effective mass. In a study by Kroonenberg et al., (1995), different mechanical models were used to calculate effective mass and other factors during the fall. Based on this study the values of effective mass were estimated to range between 17.1 and 26.2 kg, which corresponds to about 38% of the total body mass.

In the finite element simulations presented here, the effective mass was considered as a concentrated mass . The nodes corresponding to concentrated mass are located in the proximal end of femur, in the conjunction of hip and femur. Note that the effects of joint between hip and femur are not considered in this study.

Initial velocity of impact

The range of velocities associated with a sideway fall from a standing height was investigated by Van den Kroonenberg et al.(1996). The authors used a number of young healthy athletes to perform voluntary sideway fall on a thick foam mattress. The kinematic parameters were obtained by digitizing markers placed on anatomical points of interest. The mean value for vertical hip impact velocity reported for this experiment was 2.75 m/s.

In the finite element model, the velocity of impact was considered as the initial velocity of effective mass and was applied at the corresponding nodes.

The mechanical properties of the tissue

The soft tissues including skin, fat, and muscles overlying the femur and pelvic bone play an important role in dynamic analysis of impact. The mechanical characteristics of soft tissues can be expressed in term of stiffness and damping coefficients of these layers. The thickness of tissues is also important. It restricts the maximum displacement of the femur during the impact.

Robinovitch et al., (1991) performed an experiment to estimate mechanical properties of soft tissues in impact. In their experiment, subjects lay with the lateral aspect of the greater trochanter contacting a high fidelity force platform. Upon release of the brake, the level of hip reaction oscillated about a final level determined by the preset extension of a steel bias spring. In all trials a computer was used to acquire hip reaction data. The ultrasound measurement of soft tissue thickness over the grater trochanter were also acquired in each subject. To specify the properties, a simple mathematical model (mass- spring-damper) was used and both the stiffness and damping coefficients were reported for different tissues thickness, Fig.(4.17).

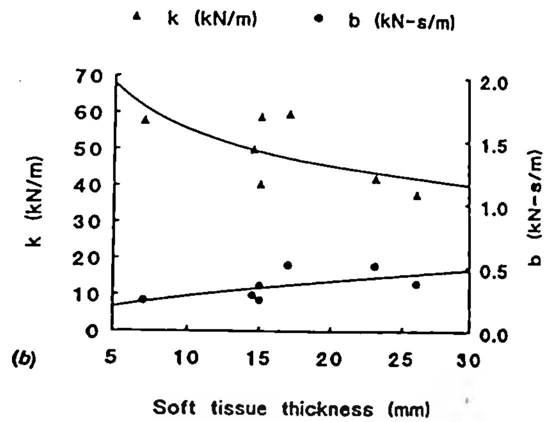

Fig.(4.17)
Stiffness and damping coefficients of soft tissues
(From: Robinovitch et al.,1991)

In the finite element model, linear springs and dampers were used to model the stiffness and damping characteristics of the tissues. The springs and dampers were located in contact area. The number of springs and dampers used in this analysis, is discussed in the section on contact area estimation ,later in this chapter.

Gap

The maximum displacement of springs, simulating the tissues, cannot exceed the soft tissues thickness in contact area. For modeling this characteristic the concept of gap was employed. A gap is defined by two nodes and the line connecting these nodes shows the gap direction. The gap distance is defined as the maximum allowable relative displacement between the two nodes along the gap direction. A gap has no effect on the response of the system when the distance between corresponding nodes is less than gap distance. However when this distance is larger than gap distance, a contact takes place.

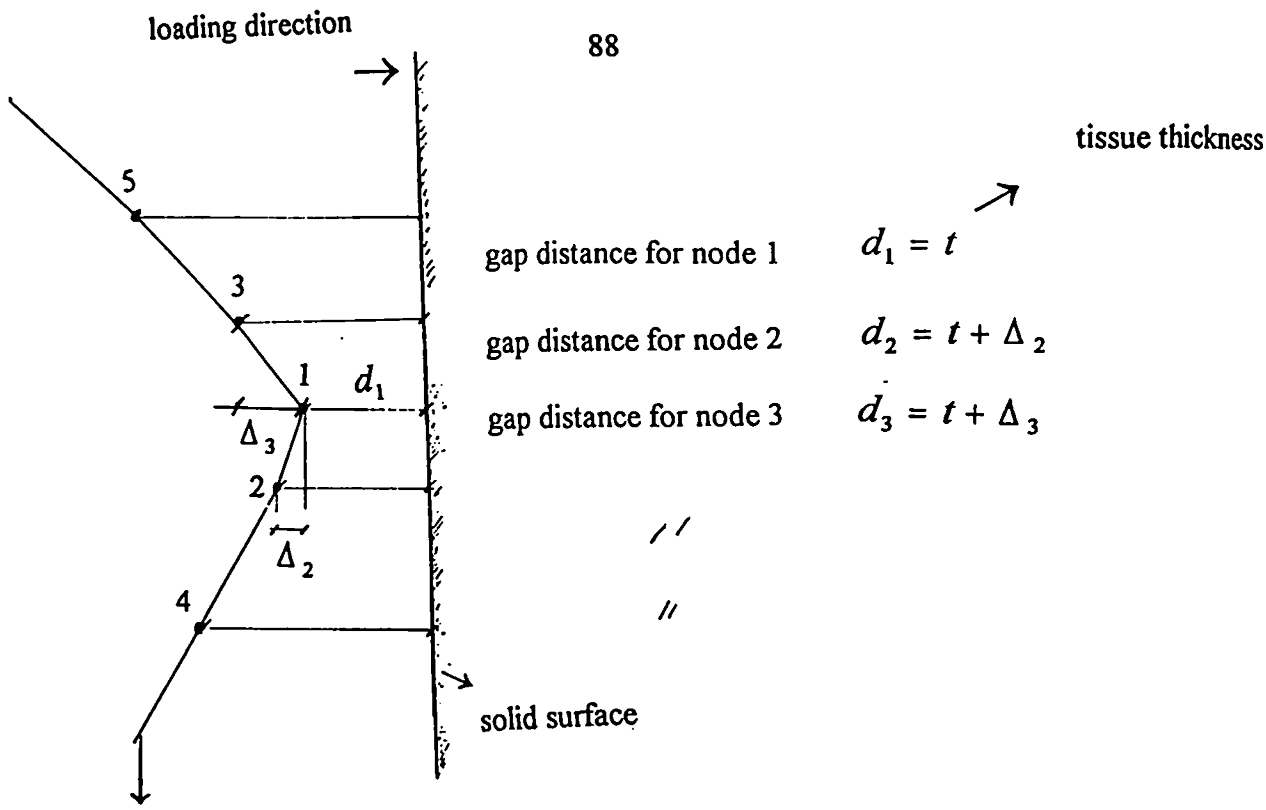

Fig.(4.18)

In this analysis gaps were defined for each of the springs, with the gap direction coinciding with initial velocity. The gap distance for each node was calculated based on a simple concept shown in Fig(4.18).

Contact area

Contact area is the area of that part of tissue which is in contact with the solid surface at the moment of impact. Estimates of contact area basically depend on the geometry of the tissue, which was not accounted for in this study. Instead, a simple approximation was used to define the number of nodes in contact, as shown in Fig(4.19).

The springs shown in the picture simulate the tissue and are located at the surface of the femur. Assuming that all of these springs have equal stiffness and knowing the total stiffness of the tissue and the maximum force of impact , it is possible to calculate the number of nodes located in contact area.

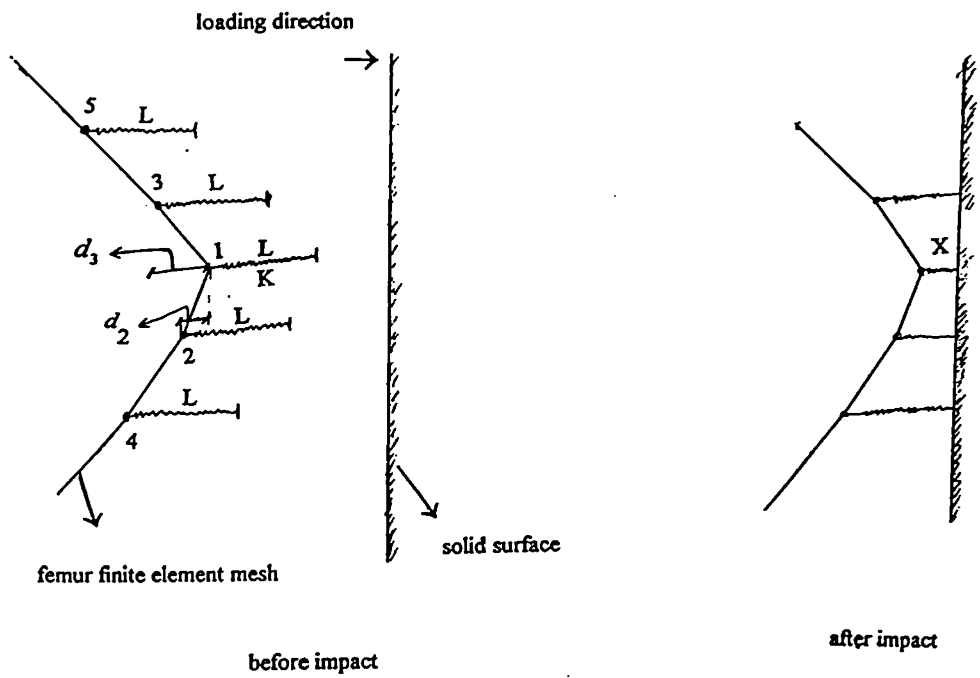

force at spring 1: $F_1 = K(L - X)$

force at spring 2: $F_2 = K(L + d_2 - X)$

force at spring 3: $F_3 = K(L + d_3 - X)$

....

total force of impact: $\sum F_i = K(nL - nX + d_2 + d_3 + \dots\dots\dots + d_n)$, $K = \frac{K_0}{n}$

n→ number of springs

K_0 → total stiffness of tissue

Fig(4.19)
Estimation of number of nodes in contact

4.4.3- Results of dynamic analysis

Dynamic analysis of fracture in proximal femur was performed for both healthy and osteoporotic bone. The results of analysis, including damage factor and mean stress distributions, are presented in figures appended at the end of this section. The details of the results are discussed below.

Fig.(4.20) is the key figure to explain the dynamics of femur fracture in a sideways fall. The figure shows time-displacement curve for one of the nodes in the contact area. The figure indicates that the node undergoes maximum displacement of 39.74 mm and then returns to its initial position. Note that at the beginning of the motion the initial velocity of femur is 2.75 m/s and when the maximum displacement is reached, at $t = 38$ ms, the velocity reduces to zero. To assess the extend of damage within the femur, different time intervals were examined. The results revealed that the maximum damage occurs at maximum displacement, i.e. at $t = 38ms$.

The results in Fig.(4.20) can also be used to determine the maximum force of impact. Given the maximum displacement of soft tissue and knowing the stiffness and total number of springs the maximum force can be calculated as:

$$F = nK\Delta \Rightarrow F = 125 \times 250 \times 0.03974 \Rightarrow F = 1242.\text{N}$$

The values of maximum displacement as well as the corresponding time of impact are close to the experimental results of Robinovitch et al.(1991) and Robinovitch et al.(1997). The estimate of maximum impact force is also very close to the results reported by Lotz et al.,(1990) and Robinovitch et al.(1991).

Fig.(4.21) shows the damage factor distribution in healthy bone (isotropic case). The distribution corresponds to the time at which maximum displacement occurs. The results are very similar to those obtained for static analysis, Fig.(4.10) and (4.11). The initiation of damage takes place in femoral neck, which is under tension.

Fig.(4.22 a) shows the midcoronal view of damage factor distribution. The distribution is again similar to that corresponding to static analysis, Fig.(4.10). Fig.(4.22 b) shows the mean stress distribution. The border between tension and compression, as well as the range of stresses, are again close to those for static analysis, Fig.(4.15).

Fig.(4.23) shows the damage factor distribution in osteoporotic bone obtained from dynamic analysis. The figure indicates that significant damage occurs in femoral neck. There is also a number of elements in contact area which are damaged. Note that dynamic analysis was performed for a linearly elastic material and nonlinearity associated with fracture may affect the distribution. Nevertheless, the results of elastic analysis are still very useful is assessing the risk of fracture.

Finally Fig.(4.24 a) shows the damage factor distribution in midcoronal plane. The extent of damage in both femoral neck and contact area is quite significant. In Fig.(4.24 b) the mean stress distribution is shown. The magnitudes of mean stresses are close to those corresponding to healthy bone, Fig.(4.22), indicating that higher damage in osteoporotic bone is due to reduction in stiffness and the strength parameters.

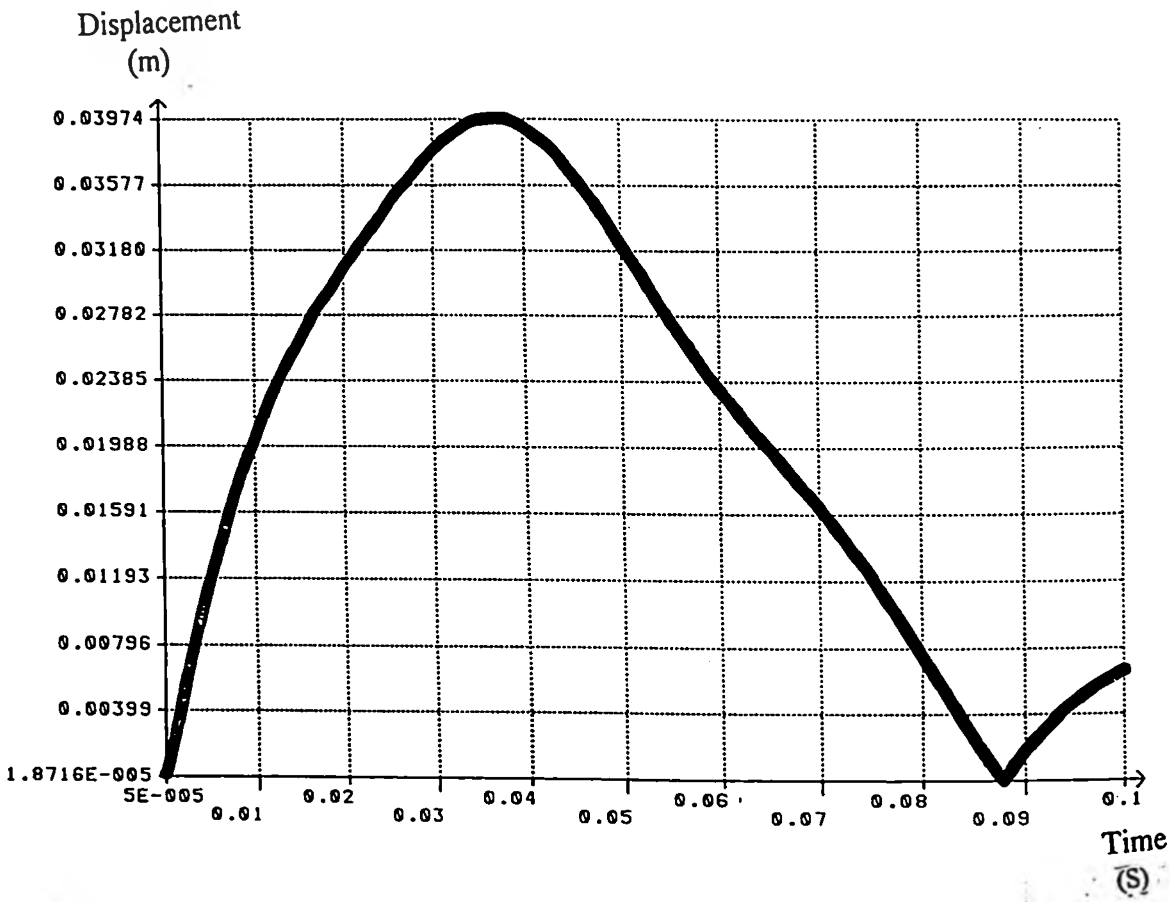

Fig.(4.20)
Time-displacement curve of a node in contact area
(Dynamic analysis)

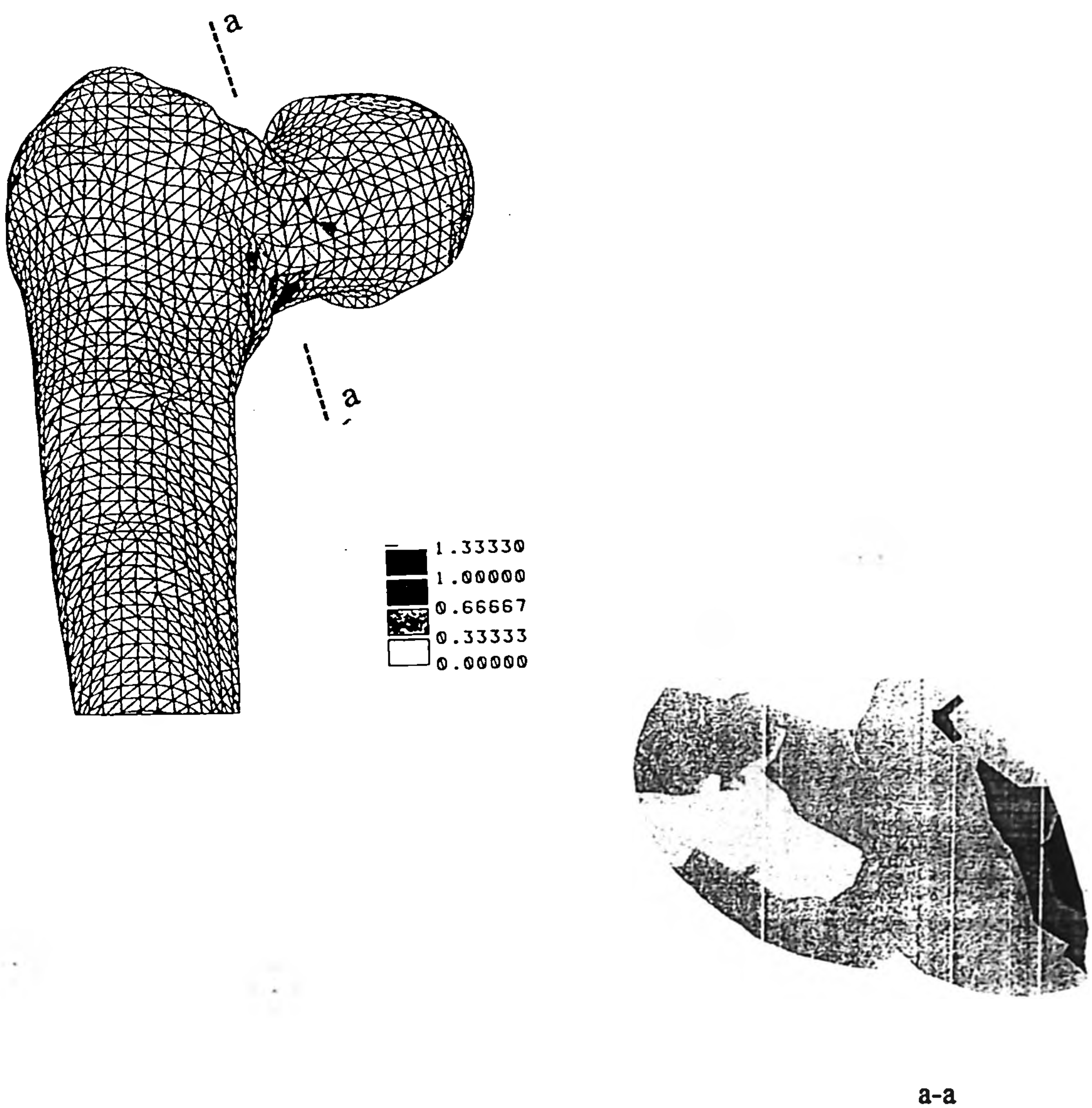

Fig.(4.21)
Damage factor (β) distribution in isotropic normal bone
(dynamic analysis)

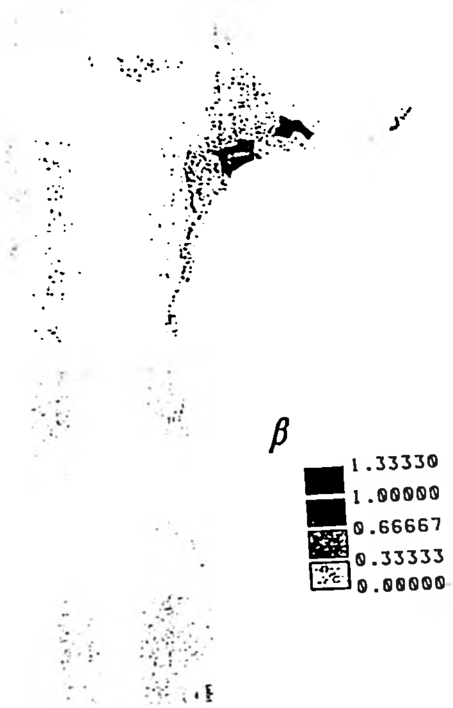

(a)

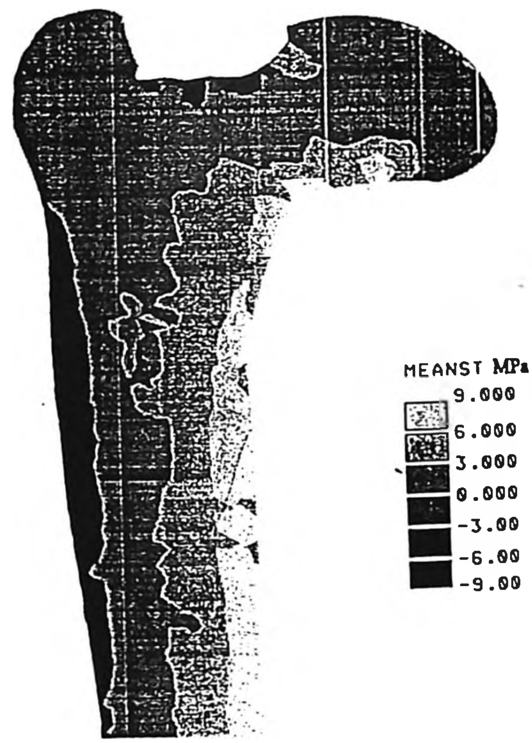

(b)

Fig.(4.22)
a)damage factor (β) distribution and b) mean stress in isotropic normal bone
(Dynamic analysis: midcoronal plane)

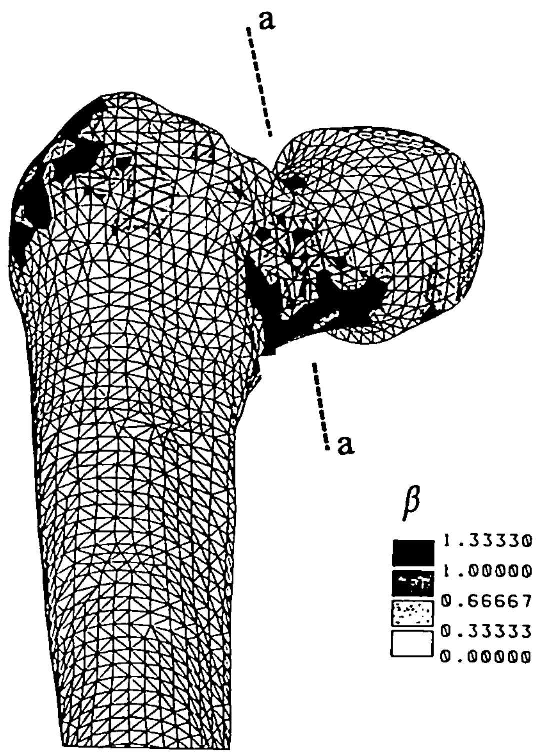

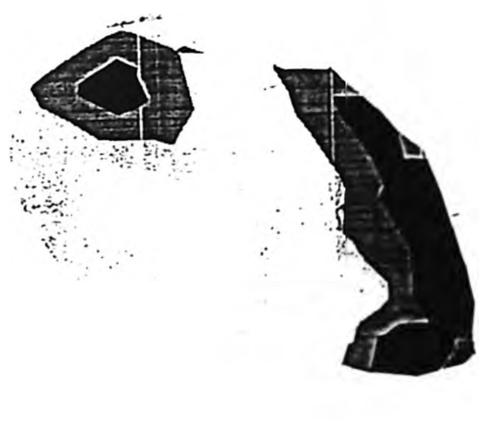

a-a

Fig.(4.23)

Damage factor (β) distribution in isotropic osteoporosis bone
(dynamic analysis)

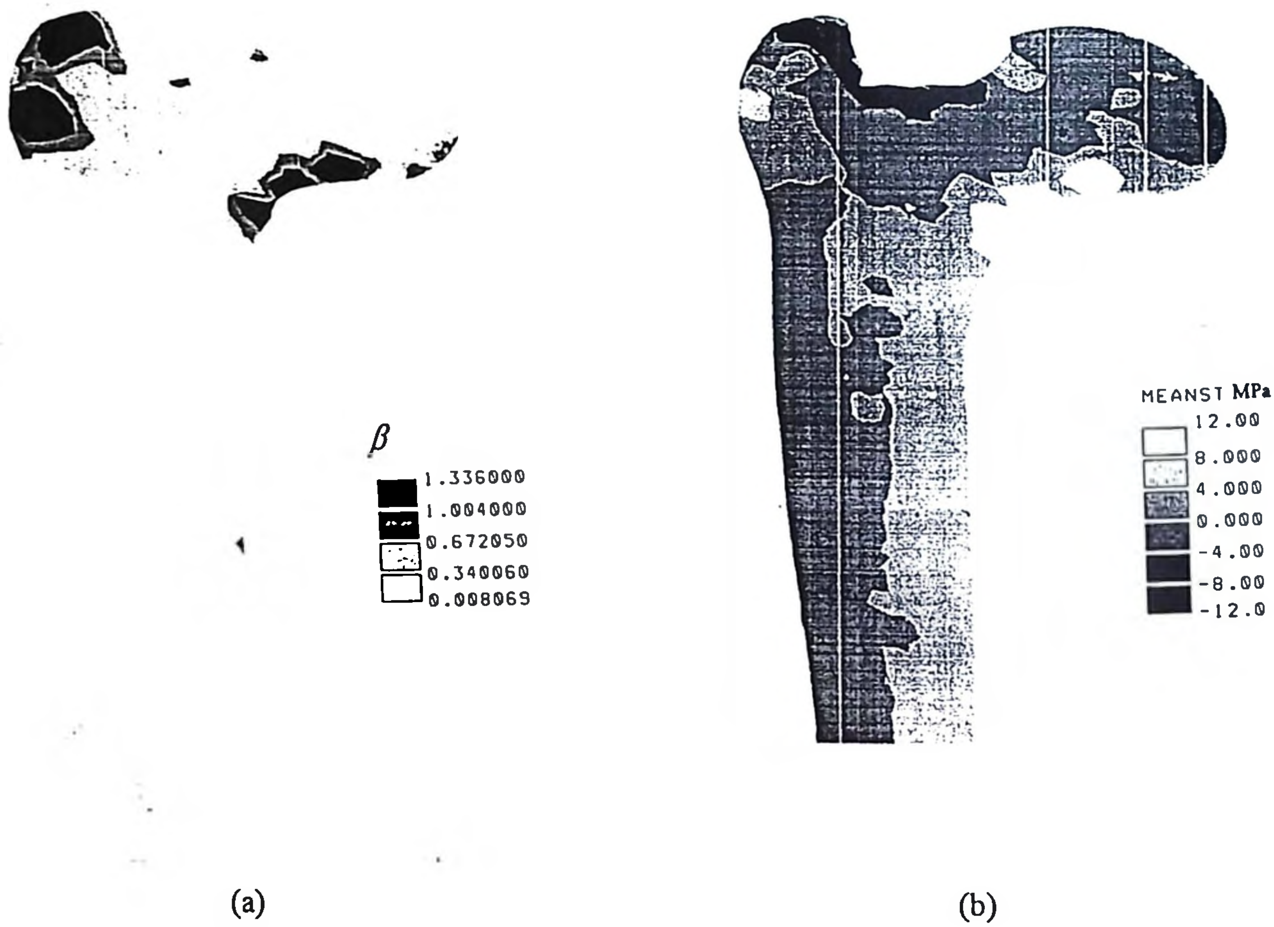

Fig.(4.24)

a)damage factor (β) distribution and b) mean stress in isotropic osteoporosis bone (Dynamic analysis: midcoronal plane)

CHAPTER 5

CONCLUSIONS AND RECOMMENDATIONS

5.1-Summary and Conclusions

The main objective of this project was to study the mechanical behavior of anisotropic porous solids. A porous solid consists of an interconnected network of solid particles and voids. The mechanical response depends on porosity, which is the primary factor affecting the material mechanical properties. The other parameters, that are commonly used to describe the orientation of material's microstructure, are called fabric tensors. A study by Pietruszczak et al. (1999a), which employs the concepts of fabric tensors, has been used in this project to define the constitutive equation and corresponding failure criteria of porous solids. The effects of liquid on the mechanical behavior of biphasic materials has also been investigated. To demonstrate the capability of the formulation, a numerical analysis of the fracture of proximal femur due to a sideways fall, which is a significant public-health problem, was performed. The analysis incorporated a finite element model developed in the work of Pietruszczak et al. (1999a) in which the geometry of femur was extracted from CT scans. The numerical analysis in this project extends the previous study in two major areas. First, a static analysis was performed, taking into the account the biphasic nature of the bone material. The second contribution concerns the extension of the analysis to dynamic range, which simulates more closely the condition of a sideways fall.

The results of both static and dynamic analysis were presented in chapter 4 . In what follows the main conclusions obtained from these results are discussed.

5.1.1- Static analysis

Isotropy & Orthotropy of bone

The results of static analysis, shown in Fig.(4.5) and (4.6), indicate that the extend of the damage is slightly higher in orthotropic material. However, the distribution of damage factor is very similar. This is primarily due to the fact that isotropic properties are taken as the orientation average corresponding to orthotropic case.

Normal and Osteoporotic bone

The higher risk of fracture in osteoporotic bone was clearly demonstrated in Fig.(4.7) to (4.9). The significant damage in osteoporotic condition is confirmed by clinical evidence which indicates higher rate of femur fractures in elderly. This is mainly due to the fact that the increase of porosity reduces the stiffness and the strength parameters in osteoporotic bone.

Dry & Biphasic properties

The results of analysis, Fig.(4.10) to Fig.(4.15), indicate that change in distribution of damage factor in dry and wet bone is not significant. The similarity results can be explained by reviewing the formulation for biphasic material. The fluid affects the behavior only when the material is under compression, and it plays no role in tension. Thus, in problems involving femur fracture, where damage occurs in tension, the significant changes in damage factor distribution are not expected.

5.1.2- Dynamic analysis

As mentioned earlier , the main purpose of dynamic analysis was to simulate more closely the conditions of a sideways fall. In the following the main conclusions of dynamic analysis are reviewed.

Maximum displacement and time of impact

Fig.(4.20) shows time-displacement curve for one of the nodes in contact area. During the impact all these nodes move towards the solid surface with an initial velocity of 2.75 m/s. Apparently, the maximum displacement can not be more than the corresponding thickness of tissues. The highest displacement obtained from time-displacement curve was 39.74 mm, which falls within the admissible range of 9-50 mm soft tissue thickness, as reported by Robinovitch et al. (1991) . The maximum displacement occurs at the time of impact of 38ms.This value is exactly the same as the experimental results reported by Robinovitch et al.,(1991) and Robinovitch et al.,(1997).

Maximum force of impact

Maximum force of impact is the highest value of force transferred to the femur during the fall. Given the maximum displacement of soft tissue and knowing the stiffness and total number of springs, the maximum force can be estimated as F=1200N. This value is very close to that reported by Lotz et al., (1990) and Robinovitch et al. (1991).

Damaged area

The distribution of damage factor for healthy and osteoporotic bone, Fig(4.21) to (4.24), is very similar to that corresponding to static analysis. The region where the highest concentration of damage occurs is located in the femoral neck. The extend of damage for healthy bone is limited, so that no fracture is expected. In osteoporotic bone, the damaged areas are significantly larger. In this case, the damage extends to regions in both tension and compression. The contours of damage factor indicate that the fracture of femur is not limited to the femoral neck but it also occurs in the region close to the contact surface. Note that the results corresponding to static analysis, Fig.(4.6 b) and Fig.(4.13 a), show no damage in the compression area. This is mainly due to the fact that, the loading configuration for static analysis is not very realistic. Comparison of the mean stress distribution in healthy and osteoporotic bone reveals that the magnitude of mean stresses is similar for both cases. This indicates that higher damage in osteoporotic bone is due to reduction in stiffness and the strength parameters.

5.2- Recommendations

The dynamic analysis of fracture of proximal femur presented in this thesis, simulates more closely the conditions of a sideway falls. However, further studies, both theoretical and experimental, are required. In what follows some suggestion and recommendation are made in this respect.

1- An extensive experimental program is required to identify the material properties of the bone in relation to material fabric. No such studies have been undertaken so far. The existing information is fragmentary and there is no correlation of properties with any measure of fabric.

2- The effect of soft tissues between pelvis and femur has been ignored in this thesis. It was primarily due to the lack of experimental data. For a more accurate analysis, the presence of these tissues should be considered.

3- The effect of tissues surrounding femur has been modeled using simple linear springs. A proper constitutive relation is required to describe the mechanical characteristics, including non-linear behavior.

4- The calculation of contact area presented in this study is very simplified. A proper contact algorithm needs to be employed for modeling the dynamic impact problem. This requires the finite element mesh discretization of both femur and the surrounding soft tissue.

The above recommendations, together with several other points suggested throughout this study, appear to be a logical continuation of present research. Upon completion of these studies, the proposed dynamic simulation may provide an efficient tool for estimation of fracture of proximal femur.

Bibliography

Backman, S., 1957, "The proximal end of the femur. Investigations with special reference to the etiology of femoral neck fractures," *Acta Radiol.* [Suppl.], Vol. 146.

Bathe, K, 1982, "Finite Element Procedures in Engineering Analysis", Prentice-Hall Inc.

Bauer, G. C. H., 1960, "Epidemiology of fracture in aged persons" A preliminary investigation in fracture Etiology. Clin. Orthop., 17:219-225, 1960.

Bohr, H., and Schaadt, O., 1983, " Bone mineral content of femoral bone and the Lumbar spine measured in women with the fracture of the femoral neck by dual photon Absorptiometry" Clin. Orthop., Vol. 179, 1983, pp. 240-245.

Burstein, A. H., Reilly, D. T., and Martens, M., 1976, "Ageing of bone tissue: Mechanical properties," *J. Bone and Joint Surg. [Am]*, Vol. 58, pp. 82-86.

Carter, D. R., and Spengler, D. M., 1978, "Mechanical properties and composition of cortical bone," *Clin. Orthop.*, Vol. 135, pp. 192-217.

Clark, J. M., and Haynor, D. R., 1987, "Anatomy of the abductor muscles of the hip as studied by computed tomography," *J. Bone and Joint Surg.*, Vol. 69-A, pp. 1021-1031.

COSMOS/M, 1996, *Finite element analysis system*, Structural Research & Analysis Corp.

Cowin, S. C, 1978, "microstructural continuum models for granular materials",in :S. C. Cowin and M. Satake, eds.,Continuum Mechanical and Statistical Approach in the Mechanics of Granular Materials, Gakujutsu Bunken,Fukyu-kai, Tokyo.

Cowin, S.C., 1979, "On the strength anisotropy of bone and wood",Mechanics of Materials 4,137

Cowin, S.C, 1981, " Mechanical properties of bone" , AMD- Vol. 45, The American Society of Mechanical Engineers.

Cowin, S.C.., 1985, "The relation between the elasticity tensor and fabric tensor", J. Biomechanics of materials 4, 137.

Cowin,S.C., 1986a, "Wolf's law of trabecular architecture at remodeling equilibrium", J. Biomechanical Engr. 108,111.

Cowin, S. C., 1986b, "Fabric dependence of an anisotropic strength criterion," *Mech. Mater.*, Vol. 5, pp. 251-260.

Cowin, S.C.., 1989, *Bone Mechanics*, CRC Press

Desai, C. S., Krempl, E., Kiousis, P. D., and Kundu, T., 1987, *Constitutive laws for engineering materials. Theory and applications - volume I*, Elsevier, New York.

Dullien, F.A.L., 1979, Porous media, Academic Press.

Elsasser, U, and Reeve, J.,1980, "Bone density measurement with computed tomography" Br. Med. Bull., Vol. 36, 1980, pp. 293-296.

Eriksson, S. A.V., and Widhe, T.L., 1988, "Bone mass in women with hip fracture" Acta Orthop. Scand., Vol. 59(1), 1988, pp. 19-23.

Gelfand, I.M., Minlos, R.A., and Shapiro, Z.Y., 1963, *Representations of the rotation and Lorentz groups and their applications,* Pergamon Press, New York.

Genant, H. K., Ettinger, B., Cann, C. E., Reiser, U., Gordon, G. S., and Kolb, F. O.,1985, "Osteoporosis: Assessment by Quantitative Computed Tomography" Orthop Clin. North Am., Vol. 16(3), 1985, pp. 557-568.

Gibson, Lorna J. and Ashby, Michael F.,1988, "Cellular Solids, structure & properties", Pergamon Press.

Goulet, R.W., Goldstien, S.A.,Ciarelli, M.J, Kuhn, J.L., Brown, M.B., Feldkamp,L.A..,1984, "The relationship between the structural and orthogonal compressive properties of trabecular bone"J Biomech. 27:375-389.

Graves, E., 1992, Detailed diagnosis and procedures, national hospital discharge survey, 1990. Vital and health statistics, series 13, no. 113. Pub. (PHS) 92-1774, U.S. Dept. of Health and Human services, Public Health Svc., National Center for Health Statistics, Hyattsville, Maryland.

Gray , H., 1995, Gray Anatomy, 38th edition,Churchill Livingstone

Harrigan, T., Carter,D.R, Mann, R.W., and Harris, W.H. ,1981, "The influence of apparent density and trabecular orientation on the elastic modulus of cancellous bone",Trans ORS 6:277.

Harrigan, T., and Mann, R.W., 1984, "Characterization of microstructural anisotropy in orthotropic materials using a second rank tensor," *J.Mat.Sci.*, vol.19, pp.761-767.

Hayes, W. C., McMahon, T. A., 1995, " Dynamic models for sideways falls from standing height" J. ofBiomechanical Engineering, Aug. 1995, Vol. 117, pp. 309-318.

Hodgskinson, R. and Currey, J, 1990, "The effect of variation in structure on the young's modulus of cancellous bone" , Proc Inst Mech Eng 204-H:115-121;

Jowsey, J.,1977, " Metabolic disease of bone" Philadelphia, W. B., Saunders Co.

Jung, M. (1973), "Pore structures and properties of materials" Proc. Int. Symp. RILEM/ UPAC, Prague, Sep. 18-21, Prague.

Lanyon, L. E., 1974, " Experimental support for the trajectorial theory of bone structure" J. of bone and joint surgery, Vol. 56, No. B, 1974, pp. 160-166.

Kanatani, Ken-Ichi, 1984a, "Distribution of directional data and fabric tensor," *Int. J. Eng. Sci.*, Vol. 22, pp. 149-161.

Kanatani, Ken-Ichi, 1984b, "Stereological determination of structural anisotropy",Int. Engr. Sci. 22,531.

Kanatani, K.,1985a, "Measurment of crack distribution in a rock mass from observation of its surfaces", Soils and Foundations, 25,77.

Kanatani, Ken-Ichi, 1985b, "Procedure for stereological estimation of structural anisotropy" Int J Eng Sci 23:587-598

Keaveny, T. M., Wachtel, E. F., Ford, C.M., and Hayes, W. C., 1994, "Differences between the tensile and compressive strengths ofbovine tibial trabecular bone depend on modulus," *J. Biomech.*, Vol. 27, pp. 1137-1146.

Keller, T. S., 1994, "Predicting the compressive mechanical behavior of bone," *J.*

Biomech., Vol. 27, pp. 1159-1168.

Keyak, J. K., Rossi, S. A., Jones, K. A., Skinner, H. B., 1997, "Prediction of femoral fracture load using automated finite element modelling" Journal of biomechanics 31, pp. 125-133.

Koch, J. C., 1917, "The laws of bone architecture" American Journal of Anatomy, Vol.21, 1917, pp. 177-298.

Kotzar, G. M., Davy, D. T., Goldberg, V. M., Heiple, K. G., Berilla, J., Heiple, K. G. Jr., Brown, R. H., and Burstein, A. H., 1991, "Telemetrized in vivo hip joint data: A report on two patients after total hip surgery," *J. Orthop. Res.*, Vol. 9, pp. 621-633.

Kuhn, J.L., Goldstien, S.A., Feldkamp, L.A., Goulet, R.W. and Jesion, G.,1990, "Evaluation of microcomputed tomography system to study trabecular bone structure" J Orthop Res 8:833-842.

Kummer, B.,1996, "Photoelastic studies on the functional structure of bone" Folia Biotheoritica , Vol. 6, 1996, pp. 31-40.

Lewinnek, G. E., Kelsey, J., White, A. A., and Kreiger, N. J.,1980, "The significance and a comparative analysis of the epidemiology of hip fractures" Clin., Orthop., 152: 35-43, 1980.

Lotz, J. C., and Hayes, W. C., 1990, "The use of quantitative computed tomography to estimate risk of fracture of the hip from fall" J. of Bone and joint surgery, Vol. 72-A, No.5, June 1990.

Lotz, J. C., Cheal, E. J., and Hayes, W. C., 1991a, " Fracture prediction for the proximal femur using finite element models: Part I - Linear analysis," *J. Biomech. Engng.*, Vol. 113, pp. 350-360.

Lotz, J. C., Cheal, E. J., and Hayes, W. C., 1991b, "Fracture prediction for the proximal femur using finite element models: Part II - Nonlinear analysis," *J. Biomech. Engng.*, Vol. 113, pp. 361-365.

Malmeisters, A.K., 1966, "Geometry of theories of strength," *Polym. Mech. (U.S.S.R.)*, Vol.2, pp. 324-332.

Mazess, R. B., Barden, H., Ettinger, B., and Schultz, E.,1988, "Bone density of radius, spine and proximal femur in osteoporosis" J. Bone Min. Res., Vol., 3, 1988, pp. 13-18.

Mazess, R. B. and Wahner, H. M.,1988, " Nuclear medicine and densitometry" Osteoprosis: Etiology, Diagnosis, and Management, B. L. Riggs and L. J. Melton, eds., Raven Press, New York, 1988, pp. 251-295.

McLeish, R. D., and Charnley, J., 1970, "Abduction forces in the one-legged stance," *J. Biomech.*, Vol. 3, pp. 191-209.

McNamara, B. P., Viceconti, M., Cristofolini, L., and Taylor, D., 1996, "Experimental and numerical pre-clinical evaluation relating to total hip arthroplasty," *Computer Methods in Biomechanics & Biomedical Engineering*, Middleton, Jones and Pande, eds., Gordon & Breach Publishers, pp. 1-10.

Melton, L. J. III, and Riggs, B. L, 1986, "Hip fracture: A disease and an accident" Current concept of bone fragility, pp. 385-389. Eds. H. K. Uhthoff and Elvira Stahl. New York, Springer, 1986.

Melton, L. J. III, and Riggs, B. L.,1987, "Epidemiology of Age-Related Fractures" The osteoporotic Syndrome: Detection, prevention, and Treatment, L. V., Avioli, ed., Grune & Stratton, Inc., Orlando, 2nd Ed, 1987, pp. 1-30.

Melton, L. J. III, Chao, E. Y. S., and Lane, J.,1988, "Biomechanical aspect of fractures" in Osteoporosis: Etiology, Diagnosis and Management, pp. 111-131. Edited by B. L. Riggs and L. J. Melton, III. New York, Raven Press, 1988.

Merz, B., Niederer, P., Müller, R., and Rüegseggar, P., 1996, "Automated finite element analysis of excised human femora based on precision-QCT," *J. Biomech. Engng.*, Vol. 118, pp. 387-390.

Meyer, G. H., 1867, "Die Architektur der Spongiosa" Archiv für anatomie, physiologie und wissenschaftliche Medizin, Reichter und DuBois-Reymonds Archiv, vol. 34, pp. 615-628.

Murray, P. D. F.,1936, "A study of development and the structure of the vertebrae skeleton, Cambridge, U. K., Cambridge University Press,1936.

Oda M.,1976, "Fabrics and their effects on the deformation behaviours of sands", Dept of Foundation Engr., Saitama University.

Oda M., Konishi,J. and Nemat-Nasser, S.,1980, "Some experimentally based fundamental results on the mechanical behaviour of granular materials",Geotechnique 30,479.

Oda M.,Nemat-Nasser, S.and Mehrabadi M.M.,1982, "A statistical study of fabric in a random assembly of spherical granules",Int. J. Numer. Anal. Meths. Geomech. 6,77.

Oda, M, 1984, "Similarity rule of crack geometry in statistically homogenous rock masses", Mechanics of Materials 3,119.

Oda, M. Suzuki, K. and Maeshibu,T.,1984, "Elastic compliance for rock like materials with random crack", Soils and Foundations 24,27.

Odgaard, A., Jensen, E.B., and Gundersen, H.J.G. 1990, "Estimation of structural anisotropy based on volume orientation" J Micros 157:149-162.

Odgaard, A., 1997, "Three-dimensional methods for quantification of cancellous bone architecture," *Bone*, Vol. 20, pp. 315-328.

Oxnard, C. E., 1972, "Tensile force in skeletal structures" J. Morph., Vol. 134, 1972, pp. 425-436.

Pauwels, F., "Bedeutung und kausale erklarung der spongiosaarchitektur in neuer auffassung" Arztl. Wschr., Vol. 3, 1948, pp. 379.

Pietruszczak, S., Jiang, J., and Mirza, F. A., 1988, "An elastoplastic constitutive model for concrete," *Int. J. Solids Struct.*, Vol. 24, pp. 705-722.

Pietruszczak, S., and Krucinski, S., 1989, "Description of anisotropic response of clays using a tensorial measure of structural disorder," *Mech. Mater.*, Vol. 8, pp. 327-249.

Pietruszczak, S., and Pande, G. N., 1994, " On the mechanics of partially saturated soils", Comput. Geotech. 12, pp. 55-71.

Pietruszczak, S., and Pande, G. N., 1995, " On the mechanical response of saturated cemented materials, Part I: Theoretical considerations" , Int. J. Num. Anal. Meth. Geomech., Vol. 19, pp. 555-562.

Pietruszczak, S., Inglis, D., and Pande, G. N., 1997b, "Modelling of the mechanical behaviour of a femur with hip prosthesis," *Comp.Meth.Biomech.&Biomed.Engng - II*, Jones, Middleton and Pande, eds., Gordon & Breach Publ., pp. 289-298.

in the causation of fractures of the femoral neck," *J. Bone and Joint Surg.* [Am], Vol. 35, pp. 367-382.

Stone, J. L., Beaupre, G. S., and Hayes, W. C., 1983, "Multiaxial strength characteriastics of trabecular bone," *J. Biomech.*, Vol. 16, pp. 743-752.

Synder, B.D., Edwards, W.T., van der Linde, J.M., White, A.A. III., and Hayes, W.C.,1989, "Steriologic assessment of trabecular structure in the lumbar vertebra body: Biomechanical implications" Trans ORS 14:265.

Takechi, H., 1977, "Trabecular architecture of the knee joint" Acta. Orthop. Scand., Vol. 48, 1977, pp. 637-681.

Taylor, M., Tanner, K. E., Freeman, M. A. R., and Yettram, A. L., 1996, "Cancellous bone stresses surrounding cemented and press fit femoral components of a Freeman hip prosthesis in relation to clinical migration", *Computer Methods in Biomechanics & Biomedical Engineering*, Middleton, Jones and Pande, eds., Gordon & Breach Publishers, pp. 47-55.

Tobin, W. J., 1968, "Further evidence and confirmation of Wolff's law of bone transformation" Part 1 an atlas of comparative anatomy of the upper end of the femur, Clin., Ortho., Vol. 56, 1968, pp. 83-103.

Torzilli, P. A., Takebe, K., Burnstein, A. H., and Heiple, K. G., 1981, "The structural properties of immature canine bone," *J. Biomech. Engng.*, Vol. 103, pp. 232-238.

Tsai, S.W. and Wu, E.M., 1971, "A general theory of strength for anisotropic materials", *J.Composite Materials*, Vol.5, pp.58-80.

Turner, C. H., and Cowin, S. C., 1988, "Errors induced by off-axis measurements of the elastic properties of bone," *J. Biomech. Engng.*, Vol. 110, pp. 213-215.

Underwood, E.E., 1970, "Quatitative steriology", Addison-Wesley.

Van den Kroonenberg, A. J., Hayes, W. C., and McMahon, T. A., 1995, " Dynamic models for sideways falls from standing height" , Journal of Biomech. Engng., Vol. 117, pp 309-318.

Van den Kroonenberg, A. J., Hayes, W. C., and McMahon, T. A., 1995, "Hip impact velocities and body configurations for voluntary falls from standing height ", Journal of Biomechanics., Vol. 29, pp 807-811.

Pietruszczak, S., 1998a, "On inelastic behaviour of anisotropic frictional materials," *Mech. Coh. Frict. Mater.*, Vol. 4, (in print).

Pietruszczak, S., 1998b, "On the description of evolutionary phenomena in bone," *Arch. Mech.* (submitted).

Pietruszczak, S., Inglis, D., and Pande, G. N., 1999a, "A fabric-dependent fracture criterion for bone" J. of Biomechanics, Vol 32, No. 10,1999, pp. 1071-1079.

Pugh, J. W., 1974, "Quantitative studies of human subchondral cancellous bone " J.Bone and Joint Surgery, Vol. 56, No. A, 1974, pp. 313-321.

Radin, E.L., Pugh, J. W., Stienberg, R S., Parker, H. G., and Rose, R. M., 1972, " Trabecular microfractures in response to stress: the possible mechanism of Wolff's law", international congress series #291 orthopaedic surgery and traumatology, 1972, pp. 59-65.

Ravak, C. S.,1980, "Mineral content of cortical bone measured by computed tomography," J. Comput. Assist. Tomogr., Vol. 4-3, 1980, pp. 342-350.

Robinovitch, S. N., Hayes, W. C., McMahon, T. A., 1991, " Prediction of femoral impact in falls on the hip" J. of Biomechanical Engineering, Vol. 113, pp. 366-374.

Reilly, D. T., and Burstein, A. H., 1975, "The elastic and ultimate properties of compact bone tissue," *J. Biomech.*, Vol. 8, pp. 393-405.

Romer, B.,1973,"Pore structures and properties of materials" Proc. Int. Symp. RILEM/ UPAC, Prague, Sep. 18-21, Prague.

Roux,W., 1895, "Gesammelte Abhandlungen uber die Entwicklungsmechanik der organismen, W. Engelmann, Leipzig.

Satake, M.,1982, "Fabric tensor in granular materials", in: P.A. Vermeer and H.J. Lugar, eds., Deformation and Failure of Granular Materials, Belkema, Rotterdam,63.

Satake, M.,1985, "Graph-theoretical approach to the mechanics of granular materials", Technology Reports 50 Tohoku University, 1.

Smith, L. D., 1953, "Hip fracture: The role of muscle contraction or intrinsic forces

Vichnin, H. H., and Batterman, S. C. (1986), "Stress analysis and failure prediction in the proximal femur and after total hip replacement", Journal of Biomech. Engng.,Vol 108, 33-41.

Wang, J.C. ,1984, "Young's modulus of porous materials".

Whitehouse, W.J., 1974, "The quantitative morphology of anisotropic trabecular bone," *J.Microsc.*, vol.101, pp.153-168.

Wolff, J.,1870, "Uber die innere Architektur der Knochen und ihre Bedeutung fur die Frage vom Knochenwachstum" Archiv fur pathologicsche Anatomie und physiologie und fur klinische Medizin, Virchous Archiv, Vol. 50, 1870, pp. 389-453.

Wolff, J., 1892, "Das gesetz der transformation der knochen, Berlin" A. Hirchwild, 1892

Zysset, P. K., and Curnier, A., 1995, "An alternative model for anisotropic elasticity based on fabric tensors," *Mech. Mater.*, Vol. 21, pp. 243-250.

Zysset, P. K., and Curnier, A., 1996, "A 3D damage model for trabecular bone based on fabric tensors," *J. Biomech.*, Vol. 29, pp. 1549-1558.